

Risk of Cascading Collisions in Network of Vehicles with Delayed Communication

Guangyi Liu, Christoforos Somarakis, and Nader Motee¹

Abstract—This work explores cascading failures in networked control systems by employing a platoon of vehicles that exchange information over a time-delayed communication graph as a model. We study the roles of network connectivity, system dynamics, communication time-delay, and uncertainty in the emergence of these failure phenomena. Our results yield closed-form expressions for the average value-at-risk (AV@R), which we utilize as a coherent risk measure to quantify the cascading effect of vehicle collisions within a platoon. These findings are further extended with several standard communication graphs with symmetries to reveal the impact of graph design parameters on the risk of cascading collisions. By presenting the boundedness of the steady-state statistics of the inter-vehicle distances, we present the best achievable risk of cascading collision with general graph topologies, which is further specified for special communication graph such as the complete graph. Our theoretical findings pave the way for the development of a robust framework designed to mitigate the risk of cascading collisions in vehicle platoons by exploring how platoon reacts to the various existing failures and the change of communication links.

I. INTRODUCTION

Uncertainties and time-delays are intrinsic elements that persistently manifest in networked control systems. The uncertainties arise from various factors, including sensor inaccuracies, environmental disturbances, and limitations in modeling the dynamic behavior of the controlled processes. Meanwhile, time-delays emerge from multiple sources, such as communication latencies, processing times, and transmission constraints. The uncertainties and time-delays in networked control systems introduce significant challenges for achieving controllability and ensuring safety: The unpredictability of system behavior due to uncertainties limits the efficacy of control strategies, potentially leading to undesired states or unstable behavior [38]. Additionally, the time-delays can disrupt the closed-loop control and compromise system stability [10]. There are numerous techniques available to measure the performance of a networked control system and assess the risk of failures in the system network. Some notable examples include studies in financial networks [1], large-scale networks [3], vehicular networks [9], power networks [4], and general networked control systems [22, 23, 25].

We explore an alternative perspective. Considering the stochastic nature of real-world systems, our working hypothesis is that faults and undesirable events are inevitable. In particular, in high-dimensional systems, even slight local

G. Liu and N. Motee are with the Department of Mechanical Engineering and Mechanics, Lehigh University, Bethlehem, PA, 18015, USA. {gliu,motee}@lehigh.edu. C. Somarakis is Senior Scientist with the Applied Mathematics Group, Merck & Co christoforos.somarakis@merck.com.

misbehavior can propagate through the system's interaction mechanisms, leading to global failure. Therefore, our focus is on studying cascading failures [19, 36, 37] in networked control systems.

From our perspective, it is essential to investigate design tools for networked control systems that can evaluate the networks' ability to contain the spread of failures occurring within network components. To accomplish this, we will develop a theoretical framework based on systemic risk analysis, with the aim of assessing the potential for cascading failures within the network. Our goal is to highlight how systemic failures in specific areas of the network can trigger additional failures across the entire system. By quantifying the impact of such failures, we can gain valuable insights into system design and recognize the vulnerabilities of networked systems to cascading failures. We will also explore the time-delay induced limitations on the systems' resilience to cascading failures as well as the potential trade-offs between the cascading failures and network connectivity. Some well known risk measures will be used for the evaluation of the resilience of the system against the cascading failures, which includes Value-at-Risk (V@R) [20] and Average Value-at-Risk (AV@R) [21, 24].

Our research focuses on examining a platoon consisting of identical autonomous vehicles that rely on a time-invariant network for communication [2, 29, 33]. However, the transmission and processing of information in the vehicles' sensors and actuators experience delays. The network is further influenced by statistical noise that affects each node independently. This noise represents external perturbations and transforms the system into a stochastic dynamical network. Our specific focus is on investigating collision events between pairs of consecutive vehicles, particularly when other pairs within the platoon have already experienced systemic failures. This paper builds upon our previous works [13, 14, 28, 7, 27] and presents a significant difference by employing AV@R as risk measures instead of the previously used V@R. Furthermore, this work considers the *cascading* effect from a single existing failure as well as multiple existing failures. We also explore the risk formulation in special graph typologies with certain symmetry and the time-delay induced fundamental limitations on the best achievable risks.

Our Contributions: To the best of our knowledge, this paper presents the first formal approach to quantifying the robustness of large-scale dynamical networks with deficiencies in the context of cascading failure events. Our preliminary findings reveal significant disparities compared to mainstream results in terms of the system components that contribute to cascading failures. This discovery serves as a motivation to redirect our research efforts towards developing methods for network design that focus on isolating existing internal failures, rather

than solely withstanding them as external disturbances. Such analysis is established in Section V by examine the AV@R of cascading failure by analyzing the steady-state distribution of a platoon of vehicles experiencing time-delayed and noisy communication. In Section VI, we investigate the contribution and interaction between pairs of vehicles within a specific graph by analyzing the marginal variance and correlation. Section VII explores the fundamental limits imposed by time-delays on the steady-state variance of the covariance, enabling us to explore the best achievable risk of cascading collisions under different conditions. Finally, in Section VIII we analyze how the communication graph topology, scale, and distribution of malfunctioning vehicles impact the risk of cascading collisions via extensive simulations.

We would like to highlight that while this work shares some similarities with the conference papers [14, 13], it presents a more thorough and nuanced examination of the effects of inter-vehicle collisions in platoons. This research incorporates novel findings and sections that were not included in the earlier conference versions. Unlike the earlier studies that used the value-at-risk measure, this study adopts the average value-at-risk measure, enhancing our understanding of the risks associated with time-delay in platoon systems. Entirely new sections, such as V-A, VI, and VII, along with a substantial part of section VIII, are introduced. The theorems and lemmas are articulated using the average value-at-risk concept, significantly reducing their overlap with the content of the previous conference versions.

II. PRELIMINARIES

The n -dimensional Euclidean space is denoted by \mathbb{R}^n and \mathbb{R}_+^n represents the non-negative orthant of \mathbb{R}^n . We denote the vector of all ones by $\mathbf{1}_n = [1, \dots, 1]^T$. The set of standard Euclidean basis for \mathbb{R}^n is represented by $\{\mathbf{e}_1, \dots, \mathbf{e}_n\}$ and $\tilde{\mathbf{e}}_i := \mathbf{e}_{i+1} - \mathbf{e}_i$ for all $i = 1, \dots, n-1$.

We consider a simple, connected, undirected, and weighted graph by \mathcal{G} , and its corresponding Laplacian matrix of \mathcal{G} is a $n \times n$ matrix $L = [l_{ij}]$ with elements

$$l_{ij} := \begin{cases} -k_{ij} & \text{if } i \neq j \\ k_{i1} + \dots + k_{in} & \text{if } i = j \end{cases},$$

where $k_{ij} \geq 0$ denotes the weight on the link (i, j) . The Laplacian matrix of a graph is symmetric and positive semi-definite [32], and the smallest Laplacian eigenvalue is zero with algebraic multiplicity one since the graph is connected. The spectrum of L can be ordered as $0 = \lambda_1 < \lambda_2 \leq \dots \leq \lambda_n$. The eigenvector that corresponds to λ_k is denoted by \mathbf{q}_k . By letting $Q = [\mathbf{q}_1 | \dots | \mathbf{q}_n]$, it follows that $L = Q\Lambda Q^T$ with $\Lambda = \text{diag}[0, \lambda_2, \dots, \lambda_n]$. We normalize the Laplacian eigenvectors such that Q becomes an orthogonal matrix, i.e., $Q^T Q = QQ^T = I_n$ with $\mathbf{q}_1 = \frac{1}{\sqrt{n}}\mathbf{1}_n$. We refer the detailed introduction of the Algebraic graph theory to the Appendix.

Let $\mathcal{L}^2(\mathbb{R}^q)$ be the set of all \mathbb{R}^q -valued random vectors $\mathbf{z} = [z^{(1)}, \dots, z^{(q)}]^T$ of a probability space $(\Omega, \mathcal{F}, \mathbb{P})$ with finite second moments. A normal random variable $\mathbf{y} \in \mathbb{R}^q$ with mean $\boldsymbol{\mu} \in \mathbb{R}^q$ and covariance matrix $\Sigma \in \mathbb{R}^{q \times q}$ is represented by $\mathbf{y} \sim \mathcal{N}(\boldsymbol{\mu}, \Sigma)$. The error function $\text{erf} : \mathbb{R} \rightarrow (-1, 1)$ is $\text{erf}(x) = \frac{2}{\sqrt{\pi}} \int_0^x e^{-t^2} dt$, which is invertible on its range as



Fig. 1: Schematics of platoon ensemble of autonomous vehicles. Speed and distance control is adjusted automatically with feedback laws using information communicated over a virtual network.

$\text{erf}^{-1}(x)$. We employ standard notation $d\xi_t$ for the formulation of stochastic differential equations.

III. PROBLEM STATEMENT

Let us consider a platoon of n vehicles along the horizontal axis as in Fig. 1, which are labeled in a descending order such that the n 'th vehicle is considered as the leader of the platoon. The state of the i 'th vehicle is denoted by $[x_t^{(i)}, v_t^{(i)}]^T$, in which $x_t^{(i)}, v_t^{(i)} \in \mathbb{R}$ represent the position and velocity of the i 'th vehicle at time t , respectively. The dynamics of the i 'th vehicle is governed by following stochastic differential equations

$$\begin{aligned} dx_t^{(i)} &= v_t^{(i)} dt \\ dv_t^{(i)} &= u_t^{(i)} dt + g d\xi_t^{(i)} \end{aligned} \quad (1)$$

where $u_t^{(i)} \in \mathbb{R}$ is the control input. We model the uncertainty in the dynamics of each vehicle with $g d\xi_t^{(i)}$, which represent the white noise generators*. It is assumed that the white noise is additive and it is independent of other vehicles' noises. The magnitude of the noise is measured by a diffusion parameter $g > 0$, and it is assumed to be identical among all vehicles. The objectives of the control of the platoon are to guarantee the following two global behaviors: (i) the pairwise differences between position variables $x_t^{(i)}$ of every two consecutive vehicles converge to 0; (ii) all vehicles attain the same velocity in the steady-state. Assuming that for any information to be communicated and processed, there is a non-negligible time-delay[†], modeled as a lumped parameter $\tau > 0$. It is known from [35] that the following feedback control law can achieve objectives (i) and (ii):

$$u_t^{(i)} = \sum_{j=1}^n k_{ij} \left(v_{t-\tau}^{(j)} - v_{t-\tau}^{(i)} \right) + \beta \sum_{j=1}^n k_{ij} \left(x_{t-\tau}^{(j)} - x_{t-\tau}^{(i)} - (j-i)r \right).$$

The parameter $\beta > 0$ balances the effect of the relative positions and the velocities in the control input and $r > 0$ denotes the target platoon distance between two consecutive vehicles. We define the vector of positions, velocities, and noise inputs as $\mathbf{x}_t = [x_t^{(1)}, \dots, x_t^{(n)}]^T$, $\mathbf{v}_t = [v_t^{(1)}, \dots, v_t^{(n)}]^T$, $\xi_t = [\xi_t^{(1)}, \dots, \xi_t^{(n)}]^T$, and the target distance vector as $\mathbf{r} = [r, 2r, \dots, nr]^T$. The feedback gain $k_{ij} \geq 0$ are designed so that the resulting communication graph stays connected.

*The stochastic process $\xi_t^{(i)} \in \mathcal{L}^2(\mathbb{R})$ denotes the real-valued Brownian motion.

[†]This assumption has been widely used by other researchers as it allows analytical derivations of formulas. For vehicle platooning, it is a common practice to use identical communication modules for all vehicles, which results in a uniform communication time-delay.

Then, the closed-loop dynamics can be cast as the following initial value problem

$$\begin{aligned} d\mathbf{x}_t &= \mathbf{v}_t dt, \\ d\mathbf{v}_t &= -L\mathbf{v}_{t-\tau} dt - \beta L(\mathbf{x}_{t-\tau} - \mathbf{r}) dt + g d\boldsymbol{\xi}_t, \end{aligned} \quad (2)$$

for all $t \geq 0$ and given deterministic values of \mathbf{x}_t and \mathbf{v}_t for $t \in [-\tau, 0]$. This poses as stochastic functional differential equations [5, 16], the standard result guarantees that $\{(\mathbf{x}_t, \mathbf{v}_t)\}_{t \geq -\tau}$ is a well-posed stochastic process.

The central *problem* studied in this work revolves around evaluating the risk of cascading failures within a platoon of vehicles, particularly in the presence of communication time-delay and exogenous noise. Our primary objective is to quantify an Average Value-at-Risk (AV@R) as a function of the communication graph Laplacian, time-delay, and noise statistics by considering scenarios where a chain of failures (of the same type) has already occurred across different locations within the system. Furthermore, we will explore the explicit formulas of the risk of cascading collisions on specific communication graphs as well as potential inherent limitations on the best achievable levels of risk.

IV. PRELIMINARY RESULTS

In this section, we provide an overview of several preliminary studies conducted to assess the stability condition of the system, examine the steady-state statistics of observables, and establish the definition of risk measures, which will serve as the foundation for the main result.

A. Internal Stability

We denote the convergence of the platoon as the velocities of all vehicles obtain the same value and the distances among all consecutive vehicles are $r > 0$, which is equivalent to

$$\lim_{t \rightarrow \infty} |v_t^{(i)} - v_t^{(j)}| = 0 \text{ and } \lim_{t \rightarrow \infty} |x_t^{(i)} - x_t^{(j)} - (i-j)r| = 0$$

for all $i, j = 1, \dots, n$. Recent works [27, 35] have shown that the deterministic platoon will converge if and only if

$$(\lambda_i \tau, \beta \tau) \in S, \quad (3)$$

for all $i = 2, \dots, n$, and we consider the set

$$S = \left\{ (s_1, s_2) \in \mathbb{R}^2 \mid s_1 \in \left(0, \frac{\pi}{2}\right), s_2 \in \left(0, \frac{a}{\tan(a)}\right), \text{ for } a \in \left(0, \frac{\pi}{2}\right) \text{ the solutions of } a \sin(a) = s_1 \right\}.$$

In this work, we only consider the cases when the deterministic platoon dynamic is convergent, i.e., $(\lambda_i \tau, \beta \tau) \in S$, where λ_i denotes the eigenvalues of the graph Laplacian matrix L .

B. Steady-State Statistics of Inter-vehicle Distances

Using the decomposition of $L = Q\Lambda Q^T$, the dynamics of the platoon (2) can be mapped into another coordinate by the state transformation

$$\mathbf{z}_t = Q^T(\mathbf{x}_t - \mathbf{r}), \text{ and } \mathbf{v}_t = Q^T \mathbf{v}_t.$$

The platoon system in the new coordinate is given by

$$\begin{aligned} d\mathbf{z}_t &= \mathbf{v}_t dt, \\ d\mathbf{v}_t &= -\Lambda \mathbf{v}_{t-\tau} dt - \beta \Lambda \mathbf{z}_{t-\tau} dt + g Q^T d\boldsymbol{\xi}_t. \end{aligned} \quad (4)$$

Once the stability condition of (4) is satisfied, the solution of decoupled subsystems can be represented as

$$\begin{bmatrix} z_t^{(i)} \\ v_t^{(i)} \end{bmatrix} = \Gamma(z_{[-\tau, 0]}; v_{[-\tau, 0]}) + g \int_0^t \Phi_i(t-s) B_i d\boldsymbol{\xi}_s, \quad (5)$$

for $\Gamma(\cdot, \cdot)$ a generalized function describing transient dynamics that vanish exponentially fast [27], and $B_i = [0_{1 \times n}, \mathbf{q}_i^T]^T$. It is known from [27] that the statistics of the steady-state $\bar{\mathbf{z}} \in \mathbb{R}^n$ follows a multi-variate normal distribution with mean $\mathbf{0}$ and the covariance matrix is shown by $\Sigma_z = \text{diag}\{\sigma_{z_1}^2, \dots, \sigma_{z_n}^2\}$, in which $\sigma_{z_i}^2 = \frac{g^2 \tau^3}{2\pi} f(\lambda_i \tau, \beta \tau)$ with

$$f(s_1, s_2) = \int_{\mathbb{R}} \frac{dr}{(s_1 s_2 - r^2 \cos(r))^2 + r^2 (s_1 - r \sin(r))^2}. \quad (6)$$

Given that $\mathbf{x}_t = Q\mathbf{z}_t + \mathbf{y}$, we define the steady-state distance vector of the platoon as $\bar{\mathbf{d}} \in \mathbb{R}^{n-1}$ such that

$$\bar{\mathbf{d}} = DQ\bar{\mathbf{z}} + r\mathbf{1}_n, \quad (7)$$

in which $D = [\tilde{\mathbf{e}}_1^T | \dots | \tilde{\mathbf{e}}_{n-1}^T]^T$ and $Q = [\mathbf{q}_1 | \dots | \mathbf{q}_n]$. The i 'th element in $\bar{\mathbf{d}}$ denotes the distance between the i 'th and $(i+1)$ 'th vehicle in the platoon.

Lemma 1. Suppose the stability condition (3) holds, the steady-state inter-vehicle distance vector $\bar{\mathbf{d}}$ follows a multi-variate normal distribution in \mathbb{R}^{n-1} such that

$$\bar{\mathbf{d}} \sim \mathcal{N}(r\mathbf{1}_{n-1}, \Sigma),$$

with the elements of $\Sigma = [\sigma_{ij}]$ is shown by

$$\sigma_{ij} = g^2 \frac{\tau^3}{2\pi} \sum_{k=2}^n (\tilde{\mathbf{e}}_i^T \mathbf{q}_k)(\tilde{\mathbf{e}}_j^T \mathbf{q}_k) f(\lambda_k \tau, \beta \tau), \quad (8)$$

for all $i, j = 1, \dots, n-1$, and $f(\cdot, \cdot)$ as in (6). We also denote the diagonal elements σ_{ii} as σ_i^2 .

Remark 1. In the case when time-delay $\tau = 0$, the expression of (8) boils down to

$$\sigma_{ij} = \frac{g^2}{2\pi} \sum_{k=2}^n (\tilde{\mathbf{e}}_i^T \mathbf{q}_k)(\tilde{\mathbf{e}}_j^T \mathbf{q}_k) \int_{\mathbb{R}} \frac{dr}{(\lambda_i \beta - r^2)^2 + r^2 \lambda_i^2}.$$

Upon observing (8), it becomes evident that the cross-correlation $\rho_{ij} = \sigma_{ij}/\sigma_i \sigma_j$ remains unaffected by the magnitude of external noise, which is denoted as g . Consequently, it can be inferred that the covariance between the relative distances of two pairs of vehicles depend on the time-delay and characteristic of the underlying communication graph.

C. Risk Measures

To assess the level of uncertainty inherent in the relative distances between vehicles, we utilize the concept of Value-at-Risk (V@R), and Average Value-at-Risk (AV@R) [6, 21, 24]. Both risk measures quantify the likelihood of a random variable falling within an undesirable range of values, such as a near-collision scenario. The set of undesirable values is known as an unsafe set and is denoted as $C \subset \mathbb{R}$. In the probability space $(\Omega, \mathcal{F}, \mathbb{P})$, the unsafe events of the random variable $y : \Omega \rightarrow \mathbb{R}$ are defined as $\{\omega \in \Omega \mid y(\omega) \in C\}$.

In practice, one can design and tailor level sets to cover a suitable neighborhood of C to characterize alarm zones as a random variable approaches C . We establish a collection of level sets $\{C_\delta \mid \delta \in [0, \infty]\}$ of C that satisfy the following conditions for any sequence $\{\delta_n\}_{n=1}^\infty$ with property $\lim_{n \rightarrow \infty} \delta_n = \infty$:

$$\begin{aligned} 1) \quad & C_{\delta_1} \subset C_{\delta_2} \text{ when } \delta_1 > \delta_2 \\ 2) \quad & \lim_{n \rightarrow \infty} C_{\delta_n} = \bigcap_{n=1}^{\infty} C_{\delta_n} = C. \end{aligned} \quad (9)$$

The Value-At-Risk V@R of a continuous random variable y is defined as [‡] as

$$\mathfrak{R}_\varepsilon := \inf \{z \mid \mathbb{P}\{y < z\} > \varepsilon\},$$

and the corresponding AV@R [21] is given by

$$\mathfrak{A}_\varepsilon := \mathbb{E}[y \mid y < \mathfrak{R}_\varepsilon],$$

where $\varepsilon \in (0, 1)$ denotes the confidence level. The value of $\sup\{\delta \geq 0 \mid \mathfrak{A}_\varepsilon \in C_\delta\}$ indicates how dangerously y can get to C as well as the expected severity when such event occurs. Following this notation, the representation of AV@R in terms of the parameter δ of level sets C_δ is defined as follows:

$$\mathcal{A}_\varepsilon := \sup \{\delta \geq 0 \mid \mathfrak{A}_\varepsilon \in C_\delta\},$$

where a smaller ε indicates a higher level of confidence on random variable y to stay away from C . The case $\mathcal{A}_\varepsilon = 0$ signifies that $\mathbb{E}[y \mid y < \mathfrak{R}_\varepsilon]$ lands on the boundary or outside of C_0 . We have $\mathcal{A}_\varepsilon > 0$ if and only if $\mathbb{E}[y \mid y < \mathfrak{R}_\varepsilon] \in C_\delta$ for some $\delta > 0$. The extreme case $\mathcal{A}_\varepsilon = \infty$ indicates that $\mathbb{E}[y \mid y < \mathfrak{R}_\varepsilon]$ is to be found inside C . Unlike the conventional definition of AV@R which is a coherent risk measure [24], the term \mathcal{A}_ε only preserves monotonicity and sub-additivity.

V. RISK OF CASCADING COLLISIONS

Let us consider that the platoon ensemble travels in a straight line, as illustrated in Fig. 1. Naturally, there is a sequential enumeration $1, \dots, n - 1$ for pairs of consecutive vehicles. Following the notation of Lemma 2, let i and j be two pairs of vehicles in the ensemble, where i 'th pair means vehicles i and $i + 1$ and so forth.

The occurrence of an inter-vehicle collision in the i 'th pair is defined by the event $\bar{d}_i \in (-\infty, 0) = C$, and its corresponding level set can be designed as follows:

$$C_\delta = \left(-\infty, h(\delta) \right),$$

[‡]Unlike the conventional definition of $\mathfrak{R}_\varepsilon := \inf \{z \mid \mathbb{P}\{y > z\} < \varepsilon\}$, we consider the other tail of the distribution in the view of collision events.

where $\delta \in [0, \infty]$. The selection of function $h : [0, \infty] \rightarrow \mathbb{R}_+$ should ensure that C_δ satisfies the properties outlined in (9). In this paper, we adopt the function $h(\delta) = \frac{r}{\delta + c}$, resulting in the following expression for the level set:

$$C_\delta = \left(-\infty, \frac{r}{\delta + c} \right),$$

where $c \geq 1$, and the visual illustration of C_δ is shown in Fig. 2. Let us discuss scenarios that exemplify a few special cases of cascading collisions based on the given information on the occurred collisions.

A. Range Information of the Single Vehicle Pair

Let us consider the situation when one has obtained the range information about the current distance of the i 'th pair, represented by $\bar{d}_i \in C_{\delta^*}$, where $C_{\delta^*} = (-\infty, \frac{r}{\delta^* + c})$. An example is when a pair of vehicles is known to be dangerously close to collision, but their exact inter-vehicle distance is unknown due to the limited measurement capability, denoted as $\bar{d}_i \in C_{\delta^*}$ with a sufficiently large δ^* . In such scenarios, the risk of cascading collisions at the j 'th pair is defined as:

$$\mathcal{A}_\varepsilon^{i,j} = \sup \left\{ \delta \geq 0 \mid \mathbb{E}[\bar{d}_j \mid \bar{d}_j < \mathfrak{R}_\varepsilon \wedge \bar{d}_i \in C_{\delta^*}] \in C_\delta \right\},$$

with

$$\mathfrak{R}_\varepsilon := \inf \left\{ z \mid \mathbb{P}\{\bar{d}_j < z \mid \bar{d}_i \in C_{\delta^*}\} > \varepsilon \right\}.$$

Theorem 1. Suppose that the platoon (2) reaches the steady-state and the distance of the i 'th pair is observed to be $\bar{d}_i \in C_{\delta^*}$. The risk of cascading collision $\mathcal{A}_\varepsilon^{i,j}$ at the j 'th pair is

$$\mathcal{A}_\varepsilon^{i,j} := \begin{cases} 0, & \text{if } \mathfrak{A}_\varepsilon^{i,j} \geq \frac{d}{c} \\ \frac{r}{\mathfrak{A}_\varepsilon^{i,j}} - c, & \text{if } 0 < \mathfrak{A}_\varepsilon^{i,j} < \frac{d}{c}, \\ \infty, & \text{if } \mathfrak{A}_\varepsilon^{i,j} \leq 0 \end{cases}$$

where the closed form representation of $\mathfrak{A}_\varepsilon^{i,j}$ is shown in the Appendix.

The above result presents the risk of cascading collision when a pair of vehicles is identified as being dangerously close to inter-vehicle collision. It is important to note that, apart from collisions, this result can be utilized to quantify the risk of cascading failures in various scenarios, e.g., vehicles detachment [27], provided that the level set C_δ is appropriately defined. Due to the lack of *exact information*, the current analysis utilizes the *best available information* and it is constrained by the implicit structure of the expression. One can deploy state estimation techniques, e.g., Kalman filter, to get a better idea of \bar{d}_i , but it is beyond the scopes of this work. Therefore, to facilitate further analysis, we will focus on a more practical and specific case in the remaining sections of this paper, which allows for a more comprehensive examination of cascading behavior.

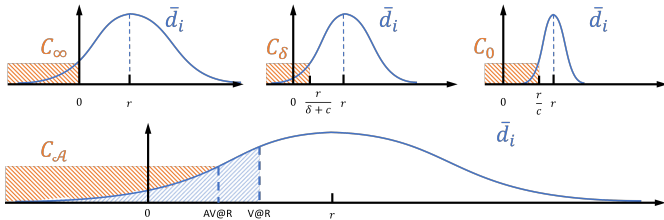


Fig. 2: Change of the set C_δ with different distributions of the inter-vehicle distance.

B. Snapshot of a Single Vehicle Pair

We now consider a special case where a single, isolated collision affects a pair of vehicles, e.g., the i 'th pair, and we have access to the measurement of its inter-vehicle distance \bar{d}_i with full precision. How does such an event affect the rest of the network? The answer follows from the closed-form expression for the statistical analysis of the steady-state distance, denoted as \bar{d}_j , when the event has occurred at the i 'th pair.

Let us assume the distance of the i 'th pair is measured as $\bar{d}_i = d^*$, and we study the risk of cascading collision at the j 'th pair in the view of the previous observation. The event of the cascading collision is defined as

$$\{\bar{d}_j \in C \mid \bar{d}_i = d^*\},$$

where $d^* \geq 0$. When $d^* = 0$, it signifies an ongoing collision at the i 'th pair. The associated risk of the cascading collision is then defined as follows:

$$\mathcal{A}_\varepsilon^{i,j} = \sup \left\{ \delta \geq 0 \mid \mathbb{E} [\bar{d}_j \mid \bar{d}_j < \mathfrak{R}_\varepsilon^{i,j} \wedge \bar{d}_i = d^*] \in C_\delta \right\}, \quad (10)$$

where

$$\mathfrak{R}_\varepsilon^{i,j} = \inf \left\{ \frac{r}{\delta + c} \mid \mathbb{P}\{\bar{d}_j \in C_\delta \mid \bar{d}_i = d^*\} > \varepsilon \right\},$$

with the confidence level $\varepsilon \in (0, 1)$. The larger value of $\mathcal{A}_\varepsilon^{i,j}$ indicates a higher probability that the cascading collision is going to occur to the system and the collision is likely to become more severe. Given the knowledge of the existing event at i , the conditional statistics at the j 'th pair is given as follows.

Lemma 2. For any pair of two steady-state distances \bar{d}_i and \bar{d}_j , the conditional distribution of $\bar{d}_j \mid \bar{d}_i = d^*$ follows a normal distribution $\mathcal{N}(\tilde{\mu}, \tilde{\sigma}^2)$, where

$$\tilde{\mu} = r + \rho_{ij} \frac{\sigma_j}{\sigma_i} (d^* - r), \text{ and } \tilde{\sigma}^2 = \sigma_j^2 (1 - \rho_{ij}^2), \quad (11)$$

in which $\rho_{ij} = \sigma_{ij}/\sigma_i \sigma_j$ and $|\rho_{ij}| < 1$. The values of σ_{ij} , σ_i , and σ_j are computed using (8).

Then, the risk of cascading collision $\mathcal{A}_\varepsilon^{i,j}$ is presented in the following result.

Theorem 2. Suppose that the platoon (2) reaches the steady-state and the i 'th pair is observed with measurement $\bar{d}_i = d^*$.

The risk of cascading collision at the j 'th pair is

$$\mathcal{A}_\varepsilon^{i,j} := \begin{cases} 0, & \text{if } \frac{c\tilde{\mu}-r}{c\tilde{\sigma}} \geq \kappa_\varepsilon \\ \frac{r}{\tilde{\mu} - \kappa_\varepsilon \tilde{\sigma}} - c, & \text{if } \kappa_\varepsilon \in (\frac{c\tilde{\mu}-r}{c\tilde{\sigma}}, \frac{\tilde{\mu}}{\tilde{\sigma}}), \\ \infty, & \text{if } \frac{\tilde{\mu}}{\tilde{\sigma}} \leq \kappa_\varepsilon \end{cases},$$

where $\kappa_\varepsilon = (\sqrt{2\pi\varepsilon} \exp(\iota_\varepsilon^2))^{-1}$, $\iota_\varepsilon = \text{erf}^{-1}(2\varepsilon - 1)$, $\tilde{\mu}$ and $\tilde{\sigma}$ are the conditional statistics computed using (11).

The above theorem presents the risk of cascading collision with branches determined by the conditional statistics of \bar{d}_i and the confidence level embedded in κ_ε . As shown in Fig. 5, there are two extreme scenarios to consider. Firstly, if $\frac{c\tilde{\mu}-r}{c\tilde{\sigma}} \geq \kappa_\varepsilon$, the there does not exists a $\delta \geq 0$ such that (10) will be satisfied. Conversely, if $\frac{\tilde{\mu}}{\tilde{\sigma}} \leq \kappa_\varepsilon$, the conditional expectation inside (10) will land outside the level set C_δ for any given $\delta \geq 0$. In any other case, the risk of cascading collision will assume a positive finite value, indicating how dangerously the AV@R of pair j is close to the collision.

We form the risk profile vector $\mathcal{A}_\varepsilon^i \in \mathbb{R}^{n-2}$ of the platoon by stacking up all risks of cascading collision among remaining pairs, such that

$$\mathcal{A}_\varepsilon^i = [\mathcal{A}_\varepsilon^{i,1}, \dots, \mathcal{A}_\varepsilon^{i,i-1}, \mathcal{A}_\varepsilon^{i,i+1}, \dots, \mathcal{A}_\varepsilon^{i,n-1}]^T.$$

Example 1: By using a path communication graph, we consider a vehicle platoon scenario on the highway, where vehicles are capable of communicating solely with their front and rear neighbors. We set $g = 0.1$, $\tau = 0.04$, and $\beta = 1$ and assume one pair of vehicles has collided, i.e., $d^* = 0$, with the result shown in Fig. 3. The risk profile reveals that the risk of cascading collisions $\mathcal{A}_\varepsilon^{i,j}$ tends to increase when the vehicles in the network gets closer to the existing collision. The results also demonstrate the risk profile when introducing an additional edge into the existing communication graph. Our findings suggest that by adding a communication link of moderate length, it becomes possible to effectively mitigate the risk of cascading collisions within the platoon.

C. Snapshots of Multiple Vehicle Pairs

The following framework enables us to consider and evaluate risk of cascading collisions when more than one single occurred collision is known.

Our goal is to quantify the risk of cascading collisions by extending Lemma 2 with utilizing the knowledge of arbitrary number of existing events. We assume that there are $m < n$ observed events in the network, labeled as $\mathcal{I}_m = i_1, \dots, i_m$. Specifically, we aim to evaluate the risk of cascading collision at the j 'th pair with $j \notin \mathcal{I}_m$. The distances of \mathcal{I}_m are represented by

$$\bar{d}_{\mathcal{I}_m} = [\bar{d}_{i_1}, \dots, \bar{d}_{i_m}]^T = \mathbf{d}^*,$$

where $\mathbf{d}^* = [d_1^*, \dots, d_m^*]^T$ corresponds to the current measurements, which can be interpreted as taking a partial snapshot of a platoon running on the highway, as depicted in Fig. 4. For example, $d_1^* = 0$ characterizes the existence of an inter-vehicle collision happening at the i_1 'th pair. Then, the risk of

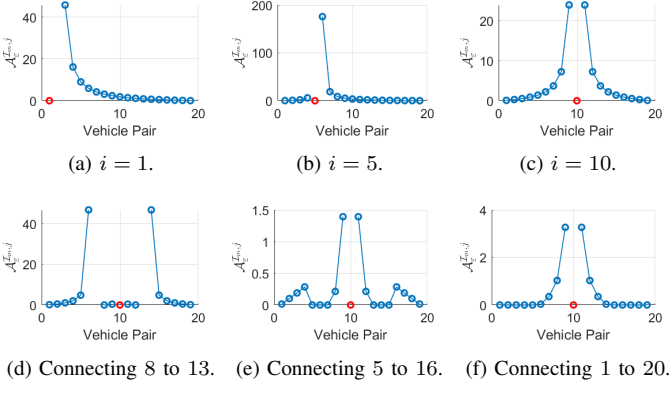


Fig. 3: The risk of cascading collision $\mathcal{A}_\varepsilon^{i,j}$ in a path graph. The second row shows the risk profile after adding an edge to the path graph.

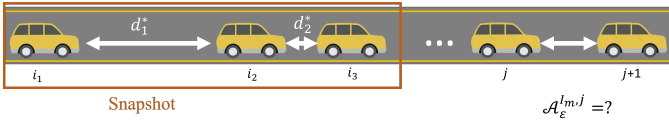


Fig. 4: The above figure illustrates the concept of snapshots of multiple vehicle pairs within a platoon.

cascading collisions at the j 'th pair is defined as

$$\mathcal{A}_\varepsilon^{\mathcal{I}_m,j} = \sup \left\{ \delta \geq 0 \mid \mathbb{E} [\bar{d}_j \mid \bar{d}_j < \mathfrak{R}_\varepsilon^{\mathcal{I}_m,j} \wedge \bar{d}_{\mathcal{I}_m} = \mathbf{d}^*] \in C_\delta \right\},$$

where

$$\mathfrak{R}_\varepsilon^{\mathcal{I}_m,j} = \inf \left\{ \frac{r}{\delta + c} \mid \mathbb{P} \{ \bar{d}_j \in C_\delta \mid \bar{d}_{\mathcal{I}_m} = \mathbf{d}^* \} > \varepsilon \right\}$$

with the confidence level $\varepsilon \in (0, 1)$. To evaluate the conditional statistics, we will consider the following block covariance matrix

$$\tilde{\Sigma} = \begin{bmatrix} \tilde{\Sigma}_{11} & \tilde{\Sigma}_{12} \\ \tilde{\Sigma}_{21} & \tilde{\Sigma}_{22} \end{bmatrix}, \quad (12)$$

where $\tilde{\Sigma}_{11} = \sigma_j^2$, $\tilde{\Sigma}_{12} = \tilde{\Sigma}_{21}^T = [\sigma_{ji_1}, \dots, \sigma_{ji_m}]$, $\tilde{\Sigma}_{22} = [\sigma_{k_1 k_2}] \in \mathbb{R}^{m \times m}$ for all $k_1, k_2 \in \mathcal{I}_m$ according to (8). Then, the conditional distribution of $\bar{d}_j \mid \bar{d}_{\mathcal{I}_m} = \mathbf{d}^*$ are shown in the following result.

Lemma 3. Suppose that $\bar{d} \sim \mathcal{N}(r\mathbf{1}_{n-1}, \Sigma)$, the conditional distribution of \bar{d}_j given $\bar{d}_{\mathcal{I}_m} = \mathbf{d}^*$ follows a normal distribution $\mathcal{N}(\tilde{\mu}, \tilde{\sigma})$, where

$$\tilde{\mu} = r - \tilde{\Sigma}_{12} \tilde{\Sigma}_{22}^{-1} (\mathbf{d}^* - r\mathbf{1}_m), \text{ and } \tilde{\sigma}^2 = \tilde{\Sigma}_{11} - \tilde{\Sigma}_{12} \tilde{\Sigma}_{22}^{-1} \tilde{\Sigma}_{21}.$$

Then, the risk of cascading collision at the j 'th pair with measurements of multiple vehicle pairs is presented as follows.

Corollary 1. Suppose that the platoon (2) reaches the steady-state and pairs with labels i_1, \dots, i_m are measured as $\bar{d}_{\mathcal{I}_m} =$

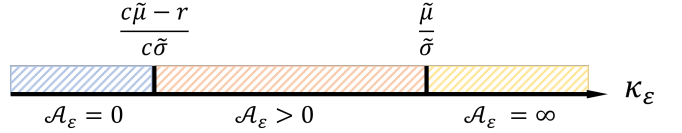


Fig. 5: The risk partition on the axis of $\kappa_\varepsilon = (\sqrt{2\pi}\varepsilon \exp(\iota_\varepsilon^2))^{-1}$.

\mathbf{d}^* . The risk of cascading collision at the j 'th pair is

$$\mathcal{A}_\varepsilon^{\mathcal{I}_m,j} := \begin{cases} 0, & \text{if } \frac{c\tilde{\mu}-r}{c\tilde{\sigma}} \geq \kappa_\varepsilon \\ \frac{r}{\gamma(\tilde{\Sigma}, \mathbf{d}^*, \varepsilon)} - c, & \text{if } \kappa_\varepsilon \in \left(\frac{c\tilde{\mu}-r}{c\tilde{\sigma}}, \frac{\tilde{\mu}}{\tilde{\sigma}} \right), \\ \infty, & \text{if } \frac{\tilde{\mu}}{\tilde{\sigma}} \leq \kappa_\varepsilon \end{cases},$$

where

$$\gamma(\tilde{\Sigma}, \mathbf{d}^*, \varepsilon) = r - \tilde{\Sigma}_{12} \tilde{\Sigma}_{22}^{-1} (\mathbf{d}^* - r\mathbf{1}_m) - \kappa_\varepsilon \sqrt{\tilde{\Sigma}_{11} - \tilde{\Sigma}_{12} \tilde{\Sigma}_{22}^{-1} \tilde{\Sigma}_{21}},$$

$\tilde{\mu}$ and $\tilde{\sigma}$ are calculated as in Lemma 3, $\kappa_\varepsilon = (\sqrt{2\pi}\varepsilon \exp(\iota_\varepsilon^2))^{-1}$, and $\iota_\varepsilon = \text{erf}^{-1}(2\varepsilon - 1)$.

The risk of a cascading collision with multiple existing events $\mathcal{A}_\varepsilon^{\mathcal{I}_m,j}$ follows a similar structure to $\mathcal{A}_\varepsilon^{i,j}$ despite the calculation of the mean and variance of the conditional distribution differs. It is important to note that the measurement of \mathcal{I}_m can take various forms. For example, in the case of multiple collisions in the platoon, one can assess the risk of cascading collisions by assuming $\bar{d}_{\mathcal{I}_m} = 0$. Alternatively, when given a partial snapshot of the platoon, the risk of collision at certain pairs can be further evaluated with this additional information. In such cases, the measurement of pairs \mathcal{I}_m do not need to be identical.

Let us also introduce the risk profile vector $\mathcal{A}_\varepsilon^{\mathcal{I}_m} \in \mathbb{R}^{n-1}$ as follows

$$\mathcal{A}_\varepsilon^{\mathcal{I}_m} = [\mathcal{A}_\varepsilon^{\mathcal{I}_m,1}, \dots, \mathcal{A}_\varepsilon^{\mathcal{I}_m,j}, \dots, \mathcal{A}_\varepsilon^{\mathcal{I}_m,n-1}]^T,$$

in which $\mathcal{A}_\varepsilon^{\mathcal{I}_m,j} = 0$ if $j \in \mathcal{I}_m$.

Example 2: We conducted experiments on a path graph with $g = 0.1$, $\tau = 0.04$, and $\beta = 1$, assuming collision occurrences between certain vehicle pairs, denoted by $\bar{d} = 0$. The obtained results are presented in Fig. 6. Our analysis indicates that as the number of existing failures increases, $\mathcal{A}_\varepsilon^{\mathcal{I}_m,j}$ tends to decrease. Additionally, the system becomes more vulnerable when the existing collisions are sparsely distributed in the platoon. Moreover, our investigation into the impact of adding an additional edge to the communication graph reveals that increasing connectivity does not always yield benefits. Instead, introducing a long-distance connection is a more favorable approach for mitigating the risk of cascading collisions.

VI. RISK OF CASCADING COLLISIONS ON SPECIAL GRAPH TOPOLOGIES

The interconnection topology of the underlying communication graph plays a crucial role in determining the extent to which uncertainties propagate in networked systems [26, 27]. In this section, we explore various graph topologies characterized by specific symmetries to gain insights into cascading failures in vehicle platooning.

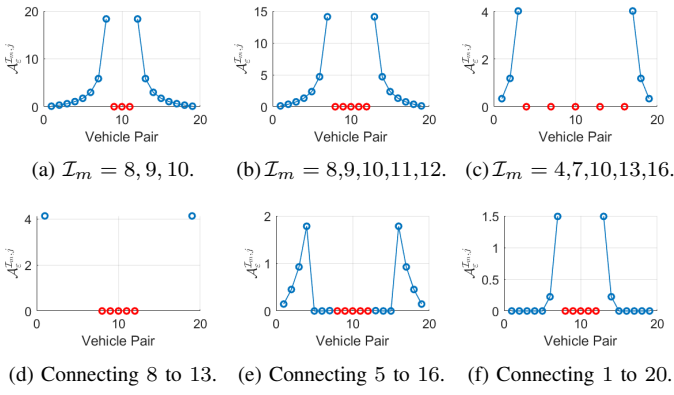


Fig. 6: The risk of cascading collision $A_e^{\mathcal{I}_m,j}$. The second row shows the risk profile after adding an edge to the path graph.

A. Complete Graph

For a platoon of vehicles (2) adopting a unweighted complete communication graph, the eigenvalues of the corresponding Laplacian matrix are: $\lambda_1 = 0$ and $\lambda_j = n$ for all $j = 2, \dots, n$. One can find the closed-form statistics of the system's observables as the following.

Lemma 4. *For a platoon (2) with a complete communication graph, the steady-state distance follows $\bar{d} \sim \mathcal{N}(r\mathbf{1}_{n-1}, \Sigma)$, and the covariance matrix is given element-wise by*

$$\sigma_{ij} := \begin{cases} \sigma_c, & \text{if } i = j \\ -\frac{\sigma_c}{2}, & \text{if } |i - j| = 1 \\ 0, & \text{if } |i - j| > 1 \end{cases}$$

where $\sigma_c = \frac{g^2 \tau^3 f(n\tau, \beta\tau)}{\pi}$ for all $i, j = 1, \dots, n - 1$.

Observing the above result, the covariance matrix Σ exhibits a distinctive symmetric tridiagonal structure, enabling the establishment of a closed-form expression for its inverse[§]. We now examine three possible scenarios regarding the relative position of the j 'th pair in relation to the existing collisions \mathcal{I}_m : (i) The j 'th pair is not adjacent to any of the collisions, (ii) The j 'th pair is only adjacent to m' consecutive collisions on one side, and (iii) The j 'th pair is surrounded by m_1 and m_2 consecutive collisions. These three scenarios are visually depicted in Fig. 7.

Let us construct a covariance matrix, denoted as $\hat{\Sigma}$, similar to the one defined in (12). However, in this case, $\hat{\Sigma}$ only considers the adjacent collisions of size \hat{m} and the j 'th pair itself, which is a square matrix of size $(\hat{m} + 1) \times (\hat{m} + 1)$. The possible values for \hat{m} are as follows: $\hat{m} = 0$ for Case (i), $\hat{m} = m'$ for Case (ii), and $\hat{m} = m_1 + m_2$ for Case (iii). In all cases, we have $m \geq \hat{m}$. We denote the inverse of the submatrix $\hat{\Sigma}_{22}$ as $\hat{\Sigma}_{22}^{-1}$, which can be represented by

[§]In this section, we specifically address collisions as the existing failures. Nevertheless, one can extend the findings to encompass other events by following the similar analogous lines of reasoning.

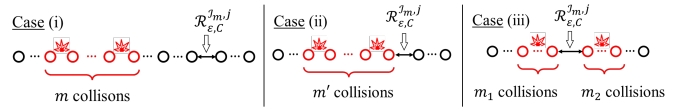


Fig. 7: This figure depicts all three cases for the relative location between failure group(s) and the pair of the interest.

the elements $[\hat{\alpha}_{ij}]$. The following result presents an analysis of the risk of cascading collision in a complete graph.

Theorem 3. *Suppose that the platoon (2) reaches the steady-state with a complete communication graph and pairs \mathcal{I}_m have experienced collisions $\bar{d}_{\mathcal{I}_m} = \mathbf{0}_m$. The risk of cascading collision at the j 'th pair is*

$$\mathcal{A}_e^{i,j} := \begin{cases} 0, & \text{if } \frac{c\hat{\mu}-r}{c\hat{\sigma}} \geq \kappa_\varepsilon \\ \frac{r}{\hat{\mu} - \kappa_\varepsilon \hat{\sigma}} - c, & \text{if } \kappa_\varepsilon \in \left(\frac{c\hat{\mu}-r}{c\hat{\sigma}}, \frac{\hat{\mu}}{\hat{\sigma}} \right), \\ \infty, & \text{if } \frac{\hat{\mu}}{\hat{\sigma}} \leq \kappa_\varepsilon \end{cases}$$

where $\kappa_\varepsilon = (\sqrt{2\pi\varepsilon} \exp(\nu_\varepsilon^2))^{-1}$, $\nu_\varepsilon = \text{erf}^{-1}(2\varepsilon - 1)$, $\hat{\mu}$ and $\hat{\sigma}$ can be computed as follows:

Case (i): If $\hat{m} = 0$, then $\hat{\mu} = r$ and $\hat{\sigma} = \sqrt{\sigma_c}$. The risk of cascading collision remains unaffected.

Case (ii): If $\hat{m} = m'$, i.e., there exists only one $k \in \mathcal{I}_m$ such that $|k - j| = 1$, one has

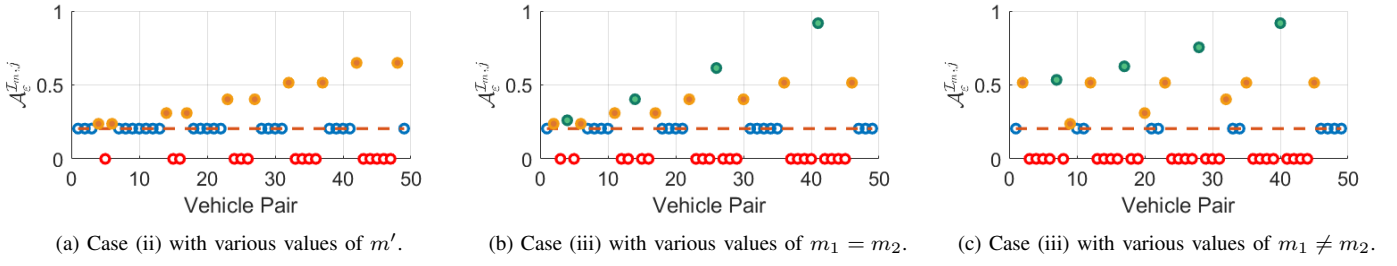
$$\hat{\sigma} = \sqrt{\sigma_j^2 - \frac{\sigma_c m'}{2(m' + 1)}}, \quad \text{and} \quad \hat{\mu} = r - \frac{\sigma_c}{2} \sum_{l=1}^{m'} \hat{\alpha}_{1,l} r.$$

Case (iii): If $\hat{m} = m_1 + m_2$, i.e., there exist $k = j - 1$ and $k' = j + 1$ for some $k, k' \in \mathcal{I}_m$, one has

$$\hat{\sigma} = \sqrt{\sigma_i^2 - \frac{\sigma_c}{2} \frac{4m_1 m_2 + m_1 + m_2}{m_1 + m_2 + 1}},$$

$$\hat{\mu} = r - \frac{\sigma_c}{2} \sum_{l=1}^{m_1+m_2} (\hat{\alpha}_{m_1,l} + \hat{\alpha}_{m_1+1,l}) r.$$

The above result indicates that when the locations of existing collisions \mathcal{I}_m are not adjacent to the j 'th pair, the level of $\mathcal{A}_e^{\mathcal{I}_m,j}$ remains unchanged compared to the risk of single collision [27]. This is due to the vanishing cross-correlation in the complete graph when the pairs are not adjacent. This observation is supported by Lemma 4 when $|i - j| > 1$, as well as by Fig. 8. In the second case, when the j 'th pair is adjacent to only one specific "group" of collisions with size m' , the magnitude of $\mathcal{A}_e^{\mathcal{I}_m,j}$ is solely determined by the dimension of the collided group. This conclusion holds regardless of whether the j 'th pair is positioned at the front or back of the collided group, see Fig. 8 (a). In the last case, the j 'th pair is situated between two distinct clusters of collisions, with sizes m_1 and m_2 respectively. The combined impact of these two collided groups contributes to the risk of cascading collisions, which, as illustrated by the green dots in Fig. 8 (b), varies based on the values of m_1 and m_2 .

Fig. 8: Risk profile $\mathcal{A}_\varepsilon^{\mathcal{I}_m,j}$ in a complete communication graph.

B. The Path Graph

If a platoon of n vehicles are using an unweighted path graph for communication, which contains n nodes and $n - 1$ edges. The eigenvalues are: $\lambda_j = 2(1 - \cos(\pi(j-1)/n))$, and their corresponding eigenvectors are shown by $\mathbf{q}_1 = \frac{1}{\sqrt{n}}\mathbf{1}_n$ and $\mathbf{q}_k = [q_k^{(1)}, \dots, q_k^{(n)}]^T$ with $q_k^{(l)} = \sqrt{\frac{2}{n}} \cos\left(\frac{\pi(n-j+1)}{2n}(2l-1)\right)$ for all $k = 2, \dots, n$ and $l = 1, \dots, n$. For the steady-state inter-vehicle distance, the elements of the covariance matrix are

$$\sigma_{ij} = \frac{4g^2\tau^3}{n\pi} \sum_{k=2}^n \theta(i, j, k) f(\lambda_k \tau, \beta \tau),$$

in which $\theta(i, j, k) = \sin\left(\frac{\pi(n-k+1)}{n}i\right) \sin\left(\frac{\pi(n-k+1)}{n}j\right) \sin^2\left(\frac{\pi(n-k+1)}{2n}\right)$. When the collision happens at the i 'th pair, the conditional distribution on the j 'th pair is given by

$$\hat{\mu} = \left(1 - \frac{\sum_{k=2}^n \theta(i, j, k) f(\lambda_k \tau, \beta \tau)}{\sum_{k=2}^n \theta(i, i, k) f(\lambda_k \tau, \beta \tau)}\right) r,$$

and

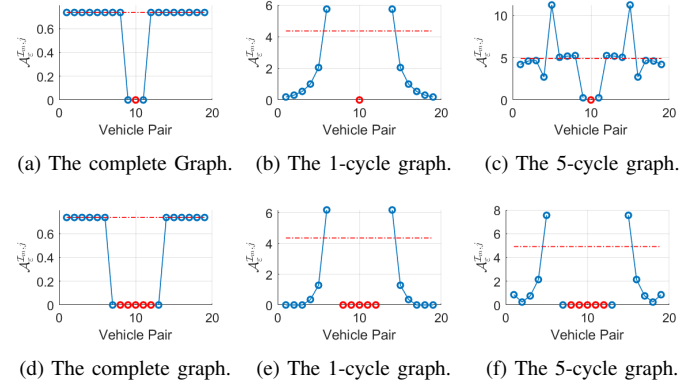
$$\hat{\sigma}^2 = \frac{4g^2\tau^3}{n\pi} \left(\sum_{k=2}^n \theta(j, j, k) f(\lambda_k \tau, \beta \tau) - \frac{(\sum_{k=2}^n \theta(i, j, k) f(\lambda_k \tau, \beta \tau))^2}{\sum_{k=2}^n \theta(i, i, k) f(\lambda_k \tau, \beta \tau)} \right).$$

The risk of cascading collisions can be evaluated using Theorem 2 or Corollary 1, and some of examples are shown in both Example 1 and 2.

C. The p -Cycle Graph

If a platoon of vehicles are using an unweighted p -cycle graph for communication, which denotes each vehicle communicates to its p -immediate neighbors. From [8, 32], one can show that eigenvalues of the corresponding Laplacian matrix are $\lambda_1 = 0$ and $\lambda_k = (\frac{\sin((2p+1)(k-1)\pi/n)}{\sin((k-1)\pi/n)} - 1)$. Their corresponding eigenvectors are shown by $\mathbf{q}_1 = \frac{1}{\sqrt{n}}\mathbf{1}_n$ and $\mathbf{q}_k = [q_k^{(1)}, \dots, q_k^{(n)}]^T$ with $q_k^{(l)} = (2p+1 - \frac{\sin((2p+1)(l-1)\pi/n)}{\sin((l-1)\pi/n)})$ for all $k \in \{2, \dots, n\}$ and $l \in \{1, \dots, n\}$. The elements of the covariance matrix Σ is shown by

$$\sigma_{ij} = \frac{g^2\tau^3}{2\pi} \sum_{k=2}^n (q_k^{(i+1)} - q_k^{(i)})(q_k^{(j+1)} - q_k^{(j)}) f(\lambda_k \tau, \beta \tau).$$

Fig. 9: The plot of the risk of cascading collision $\mathcal{A}_\varepsilon^{i,j}$. The risk profile $\mathcal{A}_\varepsilon^{\mathcal{I}_m,j}$, assuming failures occur at pairs $\{8, 9, 10, 11, 12\}$. The red dash represents the risk of collision without prior failures.

When the i 'th pair has collided, the conditional statistics of the j 'th pair is given by

$$\hat{\mu} = \left(1 - \frac{\sum_{k=2}^n (q_k^{(i+1)} - q_k^{(i)})(q_k^{(j+1)} - q_k^{(j)}) f(\lambda_k \tau, \beta \tau)}{\sum_{k=2}^n (q_k^{(i+1)} - q_k^{(i)})^2 f(\lambda_k \tau, \beta \tau)}\right) r,$$

and

$$\hat{\sigma}^2 = \frac{g^2\tau^3}{2\pi} \left(\sum_{k=2}^n (q_k^{(j+1)} - q_k^{(j)})^2 f(\lambda_k \tau, \beta \tau) - \frac{(\sum_{k=2}^n (q_k^{(i+1)} - q_k^{(i)})(q_k^{(j+1)} - q_k^{(j)}) f(\lambda_k \tau, \beta \tau))^2}{\sum_{k=2}^n (q_k^{(i+1)} - q_k^{(i)})^2 f(\lambda_k \tau, \beta \tau)} \right).$$

Then, one can compute the risk of cascading collisions as in Theorem 2 or Corollary 1.

Example 3: Some examples of using the above communication graphs are simulated with $n = 20, c = 1.1, r = 2, \tau = 0.04, \beta = 1$, and $\varepsilon = 0.1$, as shown in Fig. 9 (a) - (f). We evaluate the risk profile of cascading collision $\mathcal{A}_\varepsilon^{i,j}$ assuming that the middle pair of vehicles has collided. For multiple observed pairs, we examine vehicle pairs labeled as $\mathcal{I}_m = \{8, 9, 10, 11, 12\}$ have collided.

Complete Graph: In a complete graph, we set $g = 10$. It is shown that the immediate neighbor of an existing collision, denoted as $\mathcal{A}_\varepsilon^{i,j}$, exhibits a lower risk compared to that of

a single collision, denoted as $\mathcal{A}_\varepsilon^j$. Furthermore, the risk of cascading collisions on the remaining pairs remains unchanged when compared to $\mathcal{A}_\varepsilon^j$. When the platoon experiences multiple collisions, the adjacent vehicle pairs to the failure group demonstrates a lower risk. Furthermore, the remaining pairs share the same value as $\mathcal{A}_\varepsilon^j$, which is evident in Theorem 3.

p-Cycle Graph: We set $g = 1$ for a 1-cycle graph and $g = 10$ for a 5-cycle graph. This type of communication resemble a platoon formation model where vehicles are arranged in a loop and have the ability to communicate with their p immediate neighbors [34]. The obtained results exhibit certain properties resembling those of a complete graph. Specifically, the immediate neighbor of the collision experiences a lower $\mathcal{A}_\varepsilon^{i,j}$ compared to the risk of single collision. With smaller p values, vehicles face higher risks when they are in proximity to existing collisions. Furthermore, an interesting observation is that as the value of p increases, the risk profile exhibits a pattern more akin to that of a complete graph.

VII. TIME-DELAY INDUCED FUNDAMENTAL LIMITS ON THE RISK OF CASCADING COLLISIONS

From an engineering standpoint, one does not have the control over the communication time-delay and external disturbances. Hence, when designing the network, the focus shifts towards modifying communication topologies to achieve optimal performance and safety. In this study, our objective is to investigate the minimum achievable risk of cascading collisions for general communication topologies. We will first establish our result by initially considering the general graph topologies and then present a concrete example using the complete communication graph.

A. Fundamental Limits on the Steady-state Covariance

In this subsection, we study the boundedness of the steady-state covariance of the inter-vehicle distances on a closed and compact subset of the stability set S . We recall that $f(s_1, s_2)$ diverges on the boundary of S for $s_2 \neq 0$ where f meets its poles. On the s_1 axis, over which $s_2 = 0$ and f is finite, the dynamic of the unperturbed platoon will fail to reach the steady-state. Thus, we will consider a compact subset of S as

$$\bar{S} = [0.1, s^* \sin(s^*) - 0.1] \times [0.1, 0.9],$$

where s^* is the solution of $s^* \cot(s^*) = s_2$ for $s_2 \in [0.1, 0.9]$. One can verify that $s^* \cot(s^*) = s_2$ is invertible for $s_2 \in [0.1, 0.9]$ and can be written as $s^*(s_2)$. Then, we consider the family of all connected communication graphs such that the following condition is satisfied

$$(\lambda_i \tau, \beta \tau) \in \bar{S}, \quad (13)$$

for all $i = 2, \dots, n$.

In the following result, we will consider all the communication graphs that they satisfy $(s_1, s_2) \in \bar{S}$, and reveal the time-delay induced fundamental limits on those graphs. The following result explains time-delay induced limits on the elements of the inter-vehicles covariance matrix.

Theorem 4. For a platoon (2) with any connected communication graph that reaches the steady-state, every σ_{ij} of the steady-state covariance matrix Σ satisfies the following limits:

$$\begin{cases} \underline{\sigma} - \bar{\sigma} \leq \sigma_{ij} \leq \bar{\sigma} - \underline{\sigma}, & \text{if } |i - j| > 1 \\ \frac{1}{2}\underline{\sigma} - \frac{3}{2}\bar{\sigma} \leq \sigma_{ij} \leq \frac{1}{2}\bar{\sigma} - \frac{3}{2}\underline{\sigma}, & \text{if } |i - j| = 1 \\ 2\underline{\sigma} \leq \sigma_{ij} \leq 2\bar{\sigma}, & \text{if } |i - j| = 0 \end{cases}$$

where $\underline{\sigma} = g^2 \frac{\tau^3}{2\pi} f$, and $\bar{\sigma} = g^2 \frac{\tau^3}{2\pi} \bar{f}$. The value $\underline{f} := \inf_{(s_1, s_2) \in \bar{S}} f(s_1, s_2) \approx 25.4603$ is a lower bound of f , and $\bar{f} := \sup_{(s_1, s_2) \in \bar{S}} f(s_1, s_2) \approx 3.633 \times 10^3$ is the upper bound of f .

The above theorem establishes both upper and lower limits for the entries of the covariance matrix. It is noteworthy that these limits depend on factors such as the relative position of vehicles within the communication graph $|i - j|$, the time-delay τ , and the noise magnitude g . We highlight that the above result holds true for any connect graphs as long as it satisfies the stability condition (13).

B. A Lower Estimate of the Best Achievable Risk of Cascading Collision

Considering the time-delay and the graph connectivity induced limits on the covariance of the steady-state inter-vehicle distances, there exists limitation on the best achievable risk of cascading collisions among all feasible communication graph designs. In the following result, we provide a convenient lower estimate of the best achievable risk of cascading collision by considering the scenario featuring a single existing collision, as formulating the conditional distribution with multiple existing events introduces challenges in tracing the boundedness of the covariance terms.

Theorem 5. Suppose that the platoon (2) reaches the steady-state and the i 'th pair has collided, i.e., $d_i = 0$. Then, a lower estimate the best achievable risk of cascading collision at the j 'th is characterized as follows:

If $\sigma_{ij} > 0$,

$$\mathcal{A}_+ := \begin{cases} 0, & \text{if } 1 - \frac{\sqrt{\sigma}}{\sqrt{\sigma}} \geq \frac{1}{c} \\ \frac{\sqrt{\sigma}}{\sqrt{\sigma} - \sqrt{\sigma}} - c, & \text{if } 1 - \frac{\sqrt{\sigma}}{\sqrt{\sigma}} \in (0, \frac{1}{c}) \end{cases}.$$

If $\sigma_{ij} < 0$,

$$\mathcal{A}_- := 0.$$

If $\sigma_{ij} = 0$,

$$\mathcal{A}_0 := \begin{cases} 0, & \text{if } \frac{cr-r}{c\sqrt{2\sigma}} \geq \kappa_\varepsilon \\ \frac{r}{r - \kappa_\varepsilon \sqrt{2\sigma}} - c, & \text{if } \kappa_\varepsilon \in \left(\frac{cr-r}{c\sqrt{2\sigma}}, \frac{r}{\sqrt{2\sigma}} \right) \\ \infty, & \text{if } \frac{r}{\sqrt{\sigma}} \leq \kappa_\varepsilon \end{cases}.$$

The values of $\bar{\sigma}$ and $\underline{\sigma}$ are as in Theorem 4.

The above result presents a lower estimate of the best achievable risk of cascading collision for any communication

graphs that satisfies the stability condition (13), indicating that the risk of cascading collision can not be further optimized beyond this threshold by altering the communication graph design. Unlike the previous analyzed time-delay induced fundamental limits on the risk of single collision [27], the best achievable risk of cascading collision does not obtain a uniform value since the sign of the cross-correlation between vehicle pairs alters. This implies that when $\mathcal{A}_\varepsilon^{i,j}$ reaches its lower limit, e.g., 0, it does not indicate that the risk of cascading failure on the other vehicle will reach the same limit.

Considering the fact that the above result provides a lower estimate instead of the actual best achievable risk of cascading collision, one can not guarantee if there exists a communication graph that can reach the lower estimate. However, when designing a platoon (2) with certain constraints on the risk of cascading collision, one may consider

$$\max\{\mathcal{A}_+, \mathcal{A}_0, \mathcal{A}_-\}$$

to rule out the infeasible risk-aware design target without validating over all potential communication graphs. By imposing certain symmetry assumption to the communication graph, one can narrow down the boundedness presented in Theorem 4 and specify the best achievable risk of cascading collision in Theorem 5, as discussed in the subsequent section.

C. Best Achievable Risk of Cascading Collision on the Complete Graph

When the underlying graph is an unweighted complete graph, one can obtain the explicit formulas of σ_{ij} using Lemma 4. Then, the best achievable risk of cascading collisions can be further specified, as presented in the following result.

Corollary 2. Suppose that the platoon (2) reaches the steady-state with a complete communication graph and the i 'th pair is observed with $\bar{d}_i = d^*$. Then, the best achievable risk of cascading collision on the j 'th pair can be characterized as follows:

Case(i): If $|i - j| > 1$,

$$\mathcal{A}_\varepsilon^{i,j} \geq \begin{cases} 0, & \text{if } \frac{cr-r}{c\sqrt{2}\underline{\sigma}} \geq \kappa_\varepsilon \\ \frac{r}{r-\kappa_\varepsilon\sqrt{2}\underline{\sigma}} - c, & \text{if } \kappa_\varepsilon \in \left(\frac{cr-r}{c\sqrt{2}\underline{\sigma}}, \frac{r}{\sqrt{2}\underline{\sigma}}\right) \\ \infty, & \text{if } \frac{r}{\sqrt{2}\underline{\sigma}} \leq \kappa_\varepsilon \end{cases}$$

Case(ii): If $|i - j| = 1$,

$$\mathcal{A}_\varepsilon^{i,j} \geq \begin{cases} 0, & \text{if } \frac{c(3r-d^*)-2r}{c\sqrt{6}\underline{\sigma}} \geq \kappa_\varepsilon \\ \frac{2r}{3r-d^*-\kappa_\varepsilon\sqrt{6}\underline{\sigma}} - c, & \text{if } \kappa_\varepsilon \in \left(\frac{c(3r-d^*)-2r}{c\sqrt{6}\underline{\sigma}}, \frac{3r-d^*}{\sqrt{6}\underline{\sigma}}\right) \\ \infty, & \text{if } \frac{3r-d^*}{\sqrt{6}\underline{\sigma}} \leq \kappa_\varepsilon \end{cases}$$

where $\underline{\sigma}$ is as in Theorem 4.

The above result characterizes the best achievable risk of cascading collisions when employing a complete graph as the communication topology, while taking into account the communication time-delay and external disturbance. When $|i - j| > 1$, one can observe that the risk expression which boils down to the best achievable risk of single collision [27],

or the case when $\sigma_{ij} = 0$ in Theorem 5, since the distribution of i 'th and the j 'th vehicle are not correlated in a complete communication graph. For the case when $|i - j| = 1$, the best achievable risk can be obtained when $\sigma_c = 2\underline{\sigma}$, and such limit is uniform over among the entire platoon.

VIII. CASE STUDIES

We discuss the case studies for platoons with dynamics governed by (2) among the various communication graphs with $n = 20$, $c = 1.1$, $r = 2$, $\tau = 0.04$, $\beta = 1$, and $\varepsilon = 0.1$.

A. Impact from Failures' Proprieties

In the case only one pair of observed vehicles, the impact of the observed vehicle pair to the platoon is limited since it can only vary in either the position within the communication network or the value of the observed inter-vehicle distance. However, the impact resulting from malfunctioning vehicles becomes increasingly complex when the dimension of the failure extends beyond a single pair to *an arbitrary* number, denoted as $m < n$. One can anticipate the cascading effect is influenced by the state of the observed vehicle pairs, the spatial distribution of the affected vehicles, and the underlying communication graph topology.

1) *Dimension of Observed Vehicle Pairs:* The dimension of the measurement of observed vehicle pairs significantly impacts $\mathcal{A}_\varepsilon^{\mathcal{I}_m, j}$ due to its strong correlation with the overall uncertainty of the platoon and the conditional distribution of \bar{d}_j , both of which are functions of the value of m . In order to demonstrate this phenomenon, we consider the presence of inter-vehicle collisions ranging from 1 to 10 within the platoon. Furthermore, we analyze the risk profile across different communication graph topologies, as illustrated in Fig. 10 (a) - (e). Several noteworthy observations emerge from this analysis. Firstly, in a path graph, the overall risk escalates as the magnitude of existing failures increases. Secondly, in a complete graph, the risk of collision for the adjacent pair to the failure group \mathcal{I}_m diminishes, which aligns with the findings of Theorem 3. Thirdly, in the case of communication through a p -cycle graph, the pair situated in the middle of the functioning vehicles exhibits the highest level of safety.

2) *Spatial Distribution of the Existing Collisions:* When the scale of existing collisions is fixed for the system, the distribution of these collisions' locations significantly affects the risk profile. To assess this impact, we employ the following approach: assuming the occurrence of $m = 10$ collisions at the beginning of the platoon, and divide them into two clusters, each comprising 5 failures. Subsequently, we gradually increase the distances between these clusters, as illustrated in Fig. 13 (a) - (e). In a complete graph, it is crucial to prioritize the non-adjacent pair to \mathcal{I}_m since they obtains a higher risk of encountering the cascading collision. Alternatively, when employing a p -cycle graph, attention should be given to the pair that is close to the existing collisions. By adopting a path graph communication topology, the overall risk profile increases as the grouped failures become more spatially distributed within the platoon. Consequently, in applications involving highway platoons, it is advisable to prevent distributed collisions and rearrange the vulnerable pairs in the graph in a clustered manner.

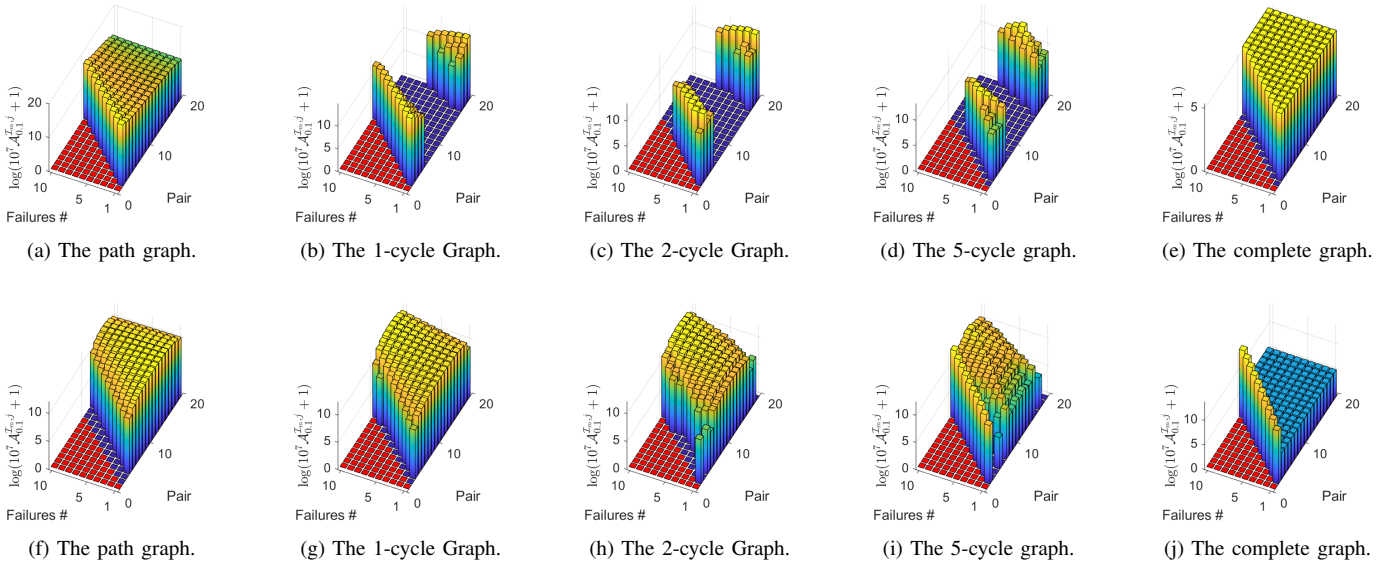


Fig. 10: Risk profile among various scale of failures and communication graphs with the red region denotes the failed vehicle pairs. The top tow resembles the risk when existing failures are collisions (0), and the bottom row represents the inter-vehicle detachment ($1.1r1_m$) [27].

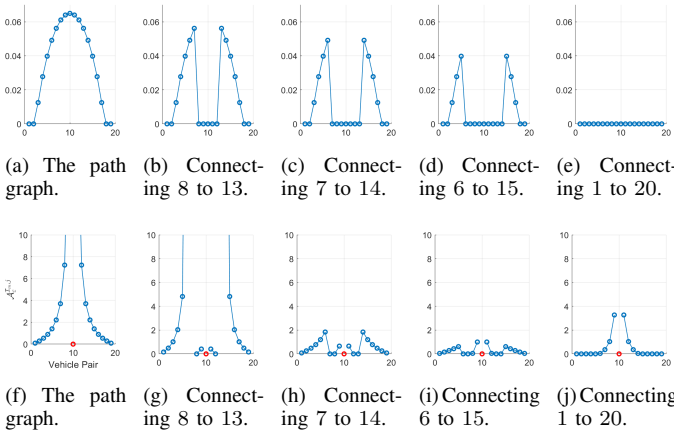


Fig. 11: Change of the risk profile when adding edges with different lengths. The first row represents the risk of single collision, and the second row represents the risk of cascading collision.

3) States of Existing Failures: In addition to our previous work [13, 14], the proposed framework expands the scope beyond considering collisions exist in the platoon, allowing for the evaluation of risk of cascading failures in various scenarios. As stated in Sec. V, the risk of cascading collisions can be evaluated with snapshots of vehicle pairs of the platoon, despite the value of the measured distances. To illustrate this concept, we simulate $\mathcal{A}_{\varepsilon}^{T_m,j}$ with $d^* = 1.1r1_m$, representing situations where pairs are widely separated rather than colliding [27], see Fig. 10 (f) - (j) and Fig. 13 (f) - (j).

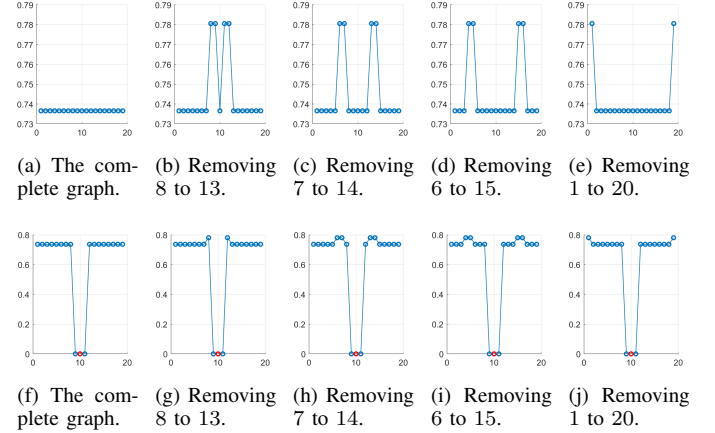


Fig. 12: Change of the risk profile when removing edges with different lengths. The first row represents the risk of single collision, and the second row represents the risk of cascading collision.

Notably, the risk profile exhibits distinct features compared to scenarios involving existing events caused by collisions. For instance, in a complete communication graph, the vehicle pairs that are close to the detached vehicles experience a higher risk of cascading collision, which is contrary to the case when some vehicles are observed colliding to each other. In a path communication graph, i.e., a highway driving scenario, our obtained results indicate that the detached pairs will reduce the risk of vehicles that are close to them, and a more spatially distributed detached pairs will reduce the overall risk

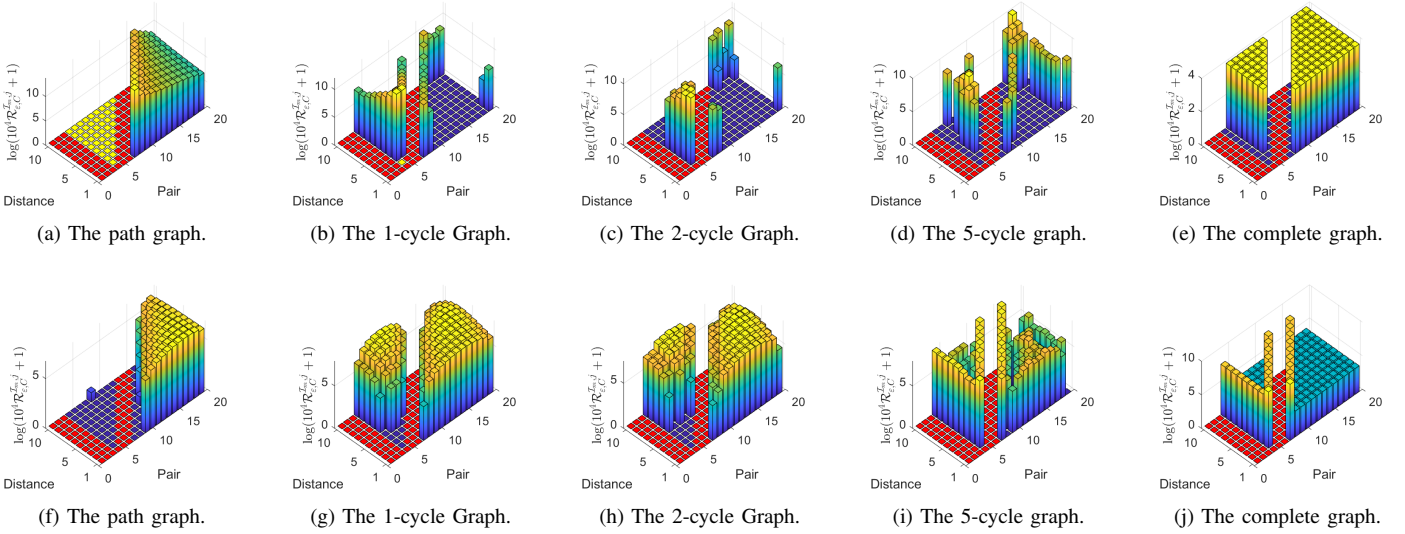


Fig. 13: Risk profile with various spatial distribution of the existing failures. The red region denotes the failed vehicle pairs and the yellow region denotes the risk reaches ∞ .

of cascading collisions for the platoon.

B. Cascading Risk-aware Communication Graph Design

In most real-world applications of vehicle platooning, the resources of reconstructing the communication graphs are limit to only adding or removing a certain links. In this section, our results provide valuable insights on how adding or removing links on standard communication graphs will impact both the risk of collision or cascading collisions in a platoon.

Adding Links: In Fig. 11, we use path graph for example with $n = 20$, $g = 0.01$, $\beta = 1$, and $\tau = 0.04$. Let us first evaluate how the risk of cascading collision might be changed when edges are added to the graph. One can observe that enhancing the local communication will does not always benefit the mitigation of the risk of cascading collision. On the other hand, the long range communication is not always the optimal solution for the path graph, indicating that the middle ranged communication is the optimal solution in this case. However, the risk of single collision obtains a different property, since increasing the length of the added communication link will always help to mitigate the risk of the single collision. Hence, it is immediate to reveal the potential trade-off between the risk of single and cascading collisions, i.e., the optimal risk profile are not obtained with the same communication graph structure for both risks and it is necessary to find the balance during the phase of communication graph design.

Removing Links: The effect of removing links is illustrated in Fig. 12, in which the complete graph is adopted for communication with $n = 20$, $g = 10$, $\beta = 1$, and $\tau = 0.04$. In the case of single collision, the complete communication graph shows an invariant property as removing edges with any length will only affect the vehicle that was connected to it, and the magnitude of the risk increment remains the same. The same

invariance also appears in the risk of cascading collisions in the complete graph, despite the length of the removed link, the increment of the risk of cascading collisions remains the same, and the rest of vehicles remains unchanged. Our finding advises that the complete communication graph is preferable in terms of robustness, as it is able to isolate and localize the impact of losing communication links.

IX. CONCLUSION AND DISCUSSION

For the time-delayed vehicle platooning problem defined in [27], we introduce the notion of the risk of cascading collisions and extend it with the average value-at-risk measure (AV@R) and with various scenarios on existing failures. We explore the properties of the cascading collision risk among several special communication graph topologies with symmetries by providing the closed-form representation of the risk of cascading collisions formula. Furthermore, we reveal and quantify the graph structure and time-delay induced limits on the risk of cascading collisions for general connected communication graphs and tighter limits on the complete graph. Our case study sheds light on the impact of existing failures, including their scale, distribution in the network, and the magnitude of the failure. From the communication graph design perspective, our result provides insight on the most advisable choice of mitigating the risk of cascading collisions when adding or removing links from the communication graphs.

The future directions of this work includes relaxing the assumption on the Gaussian input noise and investigating the distributionally robust risk of cascading collision in vehicle platooning [12, 18], and extending the current framework from point mass multiagents to multiple vehicle dynamics acting on the plane. One case study of interest is risk analysis in the dynamics of networked non-holonomic mobile vehicles for relevant formation control problems.

APPENDIX

Algebraic Graph Theory: A weighted graph is defined by $\mathcal{G} = (\mathcal{V}, \mathcal{E}, \omega)$, where \mathcal{V} is the set of nodes, \mathcal{E} is the set of edges (feedback links), and $\omega : \mathcal{V} \times \mathcal{V} \rightarrow \mathbb{R}_+$ is the weight function that assigns a non-negative number (feedback gain) to every link. Two nodes are directly connected if and only if $(i, j) \in \mathcal{E}$. Every graph \mathcal{G} is considered to be connected. In this paper, for every $i, j \in \mathcal{V}$, the following properties hold:

- $\omega(i, j) > 0$ if and only if $(i, j) \in \mathcal{E}$.
- $\omega(i, j) = \omega(j, i)$, i.e., links are undirected.
- $\omega(i, i) = 0$, i.e., links are simple.

Proof of Lemma 1: We refer to the proof of Theorem 1, [14]. \square

Proof of Theorem 1: Knowing that the steady-state distance of the i 'th pair is observed to be $\bar{d}_i \in C_{\delta^*}$, we can compute the conditional probability of $\mathbb{P}\{\bar{d}_j < \hat{d} \mid \bar{d}_i < d^*\}$ as

$$\mathbb{P}\{\bar{d}_j < \hat{d} \mid \bar{d}_i < d^*\} = \frac{\mathbb{P}\{\bar{d}_j < \hat{d} \wedge \bar{d}_i < d^*\}}{\mathbb{P}\{\bar{d}_i < d^*\}} = \frac{\int_{-\infty}^{d^*} \int_{-\infty}^{\hat{d}} h(x, y) dx dy}{\frac{1}{2} \left(1 + \text{erf}\left(\frac{x-r}{\sqrt{2}\sigma_i}\right)\right)},$$

for any $\hat{d} \in \mathbb{R}$, and $h(x, y)$ denotes the probability density function of a bi-variate normal distribution [30] such that

$$h(x, y) = \frac{\exp\left\{-\frac{1}{2(1-\rho_{ij}^2)} \left[\left(\frac{x-r}{\sigma_i}\right)^2 + \left(\frac{y-r}{\sigma_j}\right)^2 - 2\rho_{ij}\frac{(x-r)(y-r)}{\sigma_i\sigma_j} \right]\right\}}{2\pi\sigma_i\sigma_j\sqrt{1-\rho_{ij}^2}},$$

where σ_i, σ_j , and ρ_{ij} are defined in Lemma 1. Then, the $V@R$ is given by the solution of $\mathbb{P}\{\bar{d}_j < \hat{d} \mid \bar{d}_i < d^*\} = \varepsilon$ such that

$$\mathfrak{R}_{\varepsilon}^{i,j} = \text{sol} \left\{ \hat{d} \mid \int_{-\infty}^{d^*} \int_{-\infty}^{\hat{d}} h(x, y) dx dy = \frac{\varepsilon}{2} \left(1 + \text{erf}\left(\frac{x-r}{\sqrt{2}\sigma_i}\right)\right) \right\}.$$

Following the definition of $AV@R$, we have

$$\mathfrak{A}_{\varepsilon}^{i,j} = \frac{1}{\varepsilon} \frac{\int_{-\infty}^{d^*} \int_{-\infty}^{\mathfrak{R}_{\varepsilon}^{i,j}} y h(x, y) dx dy}{\frac{1}{2} \left(1 + \text{erf}\left(\frac{x-r}{\sqrt{2}\sigma_i}\right)\right)}.$$

Then, the $\mathcal{A}_{\varepsilon}^{i,j}$ can be computed by comparing the right boundary of C_{δ} with $\mathfrak{A}_{\varepsilon}^{i,j}$ which also quantifies all branches in Theorem 1. \square

Proof of Lemma 2: The result follows directly after Lemma 1 and the conditional distribution of a bi-variate normal random variable as in [30]. \square

Proof of Theorem 2: Given the fact that the continuous conditional random variable $\bar{d}_j \mid \bar{d}_i = d^*$ follows a normal distribution, $\mathbb{P}\{\bar{d}_j \mid \bar{d}_i = d^* < z\}$ can be computed as

$$\frac{1}{2} \left(1 + \text{erf}\left(\frac{z-\tilde{\mu}}{\sqrt{2}\tilde{\sigma}}\right)\right),$$

and the $V@R$ is given by

$$\mathfrak{R}_{\varepsilon}^{i,j} = \sqrt{2}\tilde{\sigma}\text{erf}^{-1}(2\varepsilon - 1) + \tilde{\mu}.$$

The corresponding $AV@R$ is evaluated by using change of variable

$$\begin{aligned} \mathfrak{A}_{\varepsilon}^{i,j} &= \frac{1}{\varepsilon} \int_{-\infty}^{\sqrt{2}\tilde{\sigma}\text{erf}^{-1}(2\varepsilon-1)+\tilde{\mu}} z \frac{1}{\sqrt{2\pi}\tilde{\sigma}} \exp\left(-\frac{(z-\tilde{\mu})^2}{2\tilde{\sigma}^2}\right) dz \\ &= \tilde{\mu} - \frac{\tilde{\sigma}}{\sqrt{2\pi\varepsilon}\exp(\tilde{\mu}^2)}, \end{aligned}$$

where $\nu_{\varepsilon} = \text{erf}^{-1}(2\varepsilon - 1)$. Then, one can conclude the result by solving for $\mathfrak{A}_{\varepsilon}^{i,j} = \frac{r}{\delta+c}$ as well as comparing $\mathfrak{A}_{\varepsilon}^{i,j}$ with 0 and $\frac{d}{c}$ to obtain branch conditions. \square

Proof of Lemma 3: The result follows directly after Lemma 1 and the conditional distribution of a multi-variate normal random variable as in [30]. \square

Proof of Corollary 1: The result can be derived using the similar lines of argument as in Theorem 2 and apply the result from Lemma 3 for the conditional statistics. \square

Proof of Lemma 4: Following Lemma 1, given that the eigenvalues λ_k are identical for all $k = 2, \dots, n$,

$$\begin{aligned} \sigma_{ij} &= \frac{g^2\tau^3 f(n\tau, \beta\tau)}{2\pi} \sum_{k=2}^n (\tilde{\epsilon}_i^T \mathbf{q}_k)(\tilde{\epsilon}_j^T \mathbf{q}_k) \\ &= \frac{g^2\tau^3 f(n\tau, \beta\tau)}{2\pi} \sum_{k=2}^n \phi(i, j, k), \end{aligned}$$

where

$$\phi(i, j, k) = (q_{k,i+1}q_{k,j+1} - q_{k,i+1}q_{k,j} - q_{k,i}q_{k,j+1} + q_{k,i}q_{k,j}),$$

and $q_{i,j}$ denotes the element of the matrix $Q = [\mathbf{q}_1 | \dots | \mathbf{q}_n]$. From the orthogonality property of the normalized eigenvectors, it is known that $\sum_k q_{k,i}q_{k,j} = \delta_{ij}$, in which δ_{ij} denotes the Kronecker delta. We have if $i = j$, then

$$\sigma_{ij} = g^2 \frac{\tau^3}{2\pi} f(n\tau, \beta\tau) (1 - 0 - 0 + 1) = \frac{1}{\pi} f(n\tau, \beta\tau) g^2 \tau^3.$$

For $|i - j| = 1$, which is equivalent to $j = i + 1$ or $i = j + 1$,

$$\sigma_{ij} = -\frac{1}{2\pi} f(n\tau, \beta\tau) g^2 \tau^3,$$

and for $|i - j| > 1$, one has $\sigma_{ij} = 0$. \square

Proof of Theorem 3: One can observe that the structure of $\tilde{\Sigma}_{22}$ is a tridiagonal matrix. Using the result from [31], considering $\theta_i = 2^{-i}\sigma_c^i(i+1)$, the inversion $\tilde{\Sigma}_{22}^{-1} = [\alpha_{ij}]$ is given by:

$$\alpha_{ij} = \begin{cases} \left(\prod_i^{j-1} \frac{\sigma_c}{2}\right) \frac{\theta_{i-1}\theta_{m-j}}{\theta_m}, & i < j \\ \frac{2i(m+1-i)}{\sigma_c(m+1)}, & i = j \\ \left(\prod_{j+1}^i \frac{\sigma_c}{2}\right) \frac{\theta_{j-1}\theta_{m-i}}{\theta_m}, & i > j \end{cases}$$

Case 1: The result is immediate since $\tilde{\Sigma}_{12} = \tilde{\Sigma}_{21}^T = [0, \dots, 0]$, the conditional mean value and the variance remains unchanged.

Case 2: Since the existing failures have no impact for the non-adjacent vehicle pairs, we only consider the adjacent failure group with size $m' \leq m$. Given that $\hat{\Sigma}_{12} = \hat{\Sigma}_{21}^T =$

$[-\sigma_c/2, 0, \dots, 0]$ or $[0, \dots, 0, -\sigma_c/2]$. Using the symmetry, the conditional variance can be written as

$$\hat{\sigma}^2 = \sigma_i^2 - \frac{\sigma_c^2}{4}\alpha_{11} = \sigma_i^2 - \frac{\sigma_c^2}{4}\alpha_{m'm'} = \sigma_i^2 - \frac{\sigma_c m'}{2(m'+1)},$$

and the value of $\hat{\mu}$ can be obtained with the same lines of argument.

Case 3: We consider the j 'th pair is between two groups with the sizes as m_1 and m_2 . Let us form a new $(m_1 + m_2) \times (m_1 + m_2)$ covariance matrix $\hat{\Sigma}$, and the rest of the result follows similarly as the previous case.

Then, one can compute $\mathcal{A}_\varepsilon^{i,j}$ using the conditional statistics evaluated above and the similar lines of argument in the proof of Theorem 2. \square

Proof of Theorem 4: Let us rewrite (8) as

$$\begin{aligned} \sigma_{ij} &= g^2 \frac{\tau^3}{2\pi} \text{Tr} (\text{diag}\{\tilde{\mathbf{e}}_i^T \mathbf{q}_1 \tilde{\mathbf{e}}_j^T \mathbf{q}_1 f(\lambda_1 \tau, \beta \tau), \dots, \\ &\quad \tilde{\mathbf{e}}_i^T \mathbf{q}_n \tilde{\mathbf{e}}_j^T \mathbf{q}_n f(\lambda_n \tau, \beta \tau)\}) \\ &= g^2 \frac{\tau^3}{2\pi} \text{Tr} (\text{diag}\{f(\lambda_1 \tau, \beta \tau), \dots, f(\lambda_n \tau, \beta \tau)\} \times \\ &\quad \text{diag}\{\tilde{\mathbf{e}}_i^T \mathbf{q}_1 \tilde{\mathbf{e}}_j^T \mathbf{q}_1, \dots, \tilde{\mathbf{e}}_i^T \mathbf{q}_n \tilde{\mathbf{e}}_j^T \mathbf{q}_n\}) \\ &= g^2 \frac{\tau^3}{2\pi} \text{Tr}(F E_{ij}) = g^2 \frac{\tau^3}{2\pi} \text{Tr}(E_{ij} F), \end{aligned}$$

where $F = \text{diag}\{f, f(\lambda_2 \tau, \beta \tau), \dots, f(\lambda_n \tau, \beta \tau)\}$, and $E_{ij} = (\tilde{\mathbf{e}}_i^T Q)^T \tilde{\mathbf{e}}_j^T Q$. Since $\tilde{\mathbf{e}}_i^T \mathbf{q}_1 \tilde{\mathbf{e}}_j^T \mathbf{q}_1 = 0$ always holds, we can set $(F)_{11} = \underline{f}$, the lowerbound of f , without loss of generality. Considering the fact that F is a normal matrix [11] in $\mathbb{R}^{n \times n}$, we can use the result from [15] (Theorem 2.10) to show

$$\sum_{i=1}^n \text{Re}(\gamma_{n-i+1}(F)) \mu_i(\bar{E}_{ij}) \leq \text{Tr}(E_{ij} F),$$

and

$$\text{Tr}(E_{ij} F) \leq \sum_{i=1}^n \text{Re}(\gamma_{n-i+1}(F)) \mu_{n-i+1}(\bar{E}_{ij}),$$

where $\gamma_i(\cdot)$ and $\mu_i(\cdot)$ denotes the i 'th eigenvalue of the matrix F and \bar{E}_{ij} in the non-decreasing order, $\bar{E}_{ij} = (E_{ij} + E_{ij}^T)/2$, and $\text{Re}(\cdot)$ denotes the real part of the eigenvalue. Let us denote by the eigenvalues of F as $\gamma_i(F)$, the smallest and the largest eigenvalue as $\gamma_{\min}(F)$ and $\gamma_{\max}(F)$. Then, the above inequality can be written as

$$\sum_{i=1}^n \gamma_i(F) \mu_i(\bar{E}_{ij}) \leq \text{Tr}(E_{ij} F) \leq \sum_{i=1}^n \gamma_i(F) \mu_{n-i+1}(\bar{E}_{ij}).$$

Considering the fact that

$$\bar{E}_{ij} = \frac{E_{ij} + E_{ij}^T}{2} = \frac{Q^T (\tilde{\mathbf{e}}_i \tilde{\mathbf{e}}_j^T + \tilde{\mathbf{e}}_j \tilde{\mathbf{e}}_i^T) Q}{2},$$

one has $\mu_i(\bar{E}_{ij}) = \mu_i(Q Q^T \frac{\tilde{\mathbf{e}}_i \tilde{\mathbf{e}}_j^T + \tilde{\mathbf{e}}_j \tilde{\mathbf{e}}_i^T}{2}) = \mu_i(\frac{\tilde{\mathbf{e}}_i \tilde{\mathbf{e}}_j^T + \tilde{\mathbf{e}}_j \tilde{\mathbf{e}}_i^T}{2})$.

By observing the structure of $\bar{E}_{ij} = \frac{\tilde{\mathbf{e}}_i \tilde{\mathbf{e}}_j^T + \tilde{\mathbf{e}}_j \tilde{\mathbf{e}}_i^T}{2}$, there exists a fixed number of rows and columns with zero entry based

on the value of $|i - j|$. Finding the eigenvalue of \bar{E}_{ij} can be simplified as follows.

Case 1: If $|i - j| = 0$, there exists $n - 2$ rows and $n - 2$ columns with zero entry such that

$$\begin{aligned} \det(\mu I_n - \bar{E}_{ij}) &= \mu^{n-2} \det \left(\mu I_2 - \begin{bmatrix} 1 & -1 \\ -1 & 1 \end{bmatrix} \right) \\ &= \mu^{n-1}(\mu - 2) = 0, \end{aligned}$$

and $\mu_1 = 2, \mu_2 = \dots = \mu_n = 0$.

Case 2: If $|i - j| = 1$, there exists $n - 3$ rows and $n - 3$ columns with zero entry and

$$\begin{aligned} \det(\mu I_n - \bar{E}_{ij}) &= \mu^{n-3} \det \left(\mu I_3 - \begin{bmatrix} 0 & 1/2 & -1/2 \\ 1/2 & 1 & 1/2 \\ -1/2 & 1/2 & 0 \end{bmatrix} \right) \\ &= \mu^{n-2}(\mu + \frac{3}{2})(\mu - \frac{1}{2}) = 0, \end{aligned}$$

and $\mu_1 = 1/2, \mu_2 = \dots = \mu_{n-1} = 0, \mu_n = -3/2$.

Case 3: If $|i - j| > 1$, there exists $n - 4$ rows and $n - 4$ columns with zero entry and

$$\begin{aligned} \det(\mu I_n - \bar{E}_{ij}) &= \mu^{n-4} \det \left(\mu I_4 - \begin{bmatrix} 0 & 0 & 1/2 & -1/2 \\ 0 & 0 & -1/2 & 1/2 \\ 1/2 & -1/2 & 0 & 0 \\ -1/2 & 1/2 & 0 & 0 \end{bmatrix} \right) \\ &= \mu^{n-2}(\mu + 1)(\mu - 1) = 0, \end{aligned}$$

and $\mu_1 = \mu_n = 1, \mu_2 = \dots = \mu_{n-1} = 0$. Then, by considering the fact that $\gamma_{\min}(F) \geq \underline{f}$ and $\gamma_{\max}(F) \leq \bar{f}$ for the closed and compact subset \bar{S} , one can conclude the result. \square

Proof of Theorem 5: Considering the fact that the risk of cascading collisions $\mathcal{A}_\varepsilon^{i,j}$ is a monotone function with respect to \mathfrak{A}_ε when it takes nonnegative finite values, one can obtain the best achievable risk by evaluating the upper limit of \mathfrak{A}_ε . When $\bar{d}_i = 0$, using the result from Lemma 2 and Theorem 2, one can write \mathfrak{A}_ε as a function of $\sigma_i, \sigma_j, \sigma_{ij}$ such that

$$\mathfrak{A}_\varepsilon(\sigma_i, \sigma_j, \sigma_{ij}) = r - r \frac{\sigma_{ij}}{\sigma_i^2} - \kappa_\varepsilon \sqrt{\sigma_j^2 - \frac{\sigma_{ij}^2}{\sigma_i^2}}$$

where $\kappa_\varepsilon > 0$. Considering the fact that $\sigma_i, \sigma_j, \sigma_{ij}$, obtained from (11), are coupled through the graph structure, let us denote the set of all feasible combinations of the triplet $(\sigma_i, \sigma_j, \sigma_{ij})$ by \mathbb{W}_G . The result from Theorem 4 also quantifies a feasible range for the triplet by

$$\mathbb{W} := \left\{ (\sigma_i, \sigma_j, \sigma_{ij}) : \sigma_i, \sigma_j \in \mathbb{W}_r, \sigma_{ij} \in (\max\{-\sigma_i \sigma_j, \underline{\sigma}_{\text{cov}}\}, \min\{\sigma_i \sigma_j, \bar{\sigma}_{\text{cov}}\}) \right\},$$

with $\mathbb{W}_r = [\sqrt{2\underline{\sigma}}, \sqrt{2\bar{\sigma}}]$, $\underline{\sigma}_{\text{cov}}$ and $\bar{\sigma}_{\text{cov}}$ denotes the limits of σ_{ij} depending on the values of $|i - j|$ as shown in Theorem 4, respectively. One can show that $\mathbb{W}_G \subset \mathbb{W}$ since \mathbb{W} is not coupled through the graph structure. Knowing that \mathfrak{A}_ε is continuous and bounded over \mathbb{W} , we have

$$\sup_{(\sigma_i, \sigma_j, \sigma_{ij}) \in \mathbb{W}_G} \mathfrak{A}_\varepsilon \leq \sup_{(\sigma_i, \sigma_j, \sigma_{ij}) \in \mathbb{W}} \mathfrak{A}_\varepsilon.$$

To facilitate the analysis, we will then consider the best achievable $\mathcal{A}_\varepsilon^{i,j}$ among \mathbb{W} . Knowing that the function $\mathfrak{A}_\varepsilon(\sigma_i, \sigma_j, \sigma_{ij})$

is continuous and differentiable functions of $\sigma_i > 0$, $\sigma_j > 0$, and $\sigma_{ij} \in (-\sigma_i\sigma_j, \sigma_i\sigma_j)$, the gradient of \mathfrak{A}_ε is computed as

$$\nabla(\mathfrak{A}_\varepsilon) = \left[\frac{\partial \mathfrak{A}_\varepsilon}{\partial \sigma_i}, \frac{\partial \mathfrak{A}_\varepsilon}{\partial \sigma_j}, \frac{\partial \mathfrak{A}_\varepsilon}{\partial \sigma_{ij}} \right]^T.$$

Observing that the term $\frac{\partial \mathfrak{A}_\varepsilon}{\partial \sigma_j} = -\frac{\kappa_\varepsilon \sigma_j}{\sqrt{\sigma_j^2 - \sigma_{ij}^2}/\sigma_i^2}$ is strictly negative for all $\sigma_j \in \mathbb{W}_r$, the first-order optimality condition [17] will not be satisfied within \mathbb{W} , indicating that the extreme values will only be obtained on the boundary of \mathbb{W} , which is given by

$$\begin{aligned} & \left\{ (\sigma_i, \sigma_j, \sigma_{ij}) : \{\sigma_i = \sqrt{2\underline{\sigma}} \text{ or } \sqrt{2\bar{\sigma}}\} \cup \{\sigma_j = \sqrt{2\underline{\sigma}} \text{ or } \sqrt{2\bar{\sigma}}\} \right\} \cap \mathbb{W}. \\ & \cup \left\{ \sigma_{ij} = \max\{-\sigma_i\sigma_j, \underline{\sigma}_{\text{cov}}\} \text{ or } \min\{\sigma_i\sigma_j, \bar{\sigma}_{\text{cov}}\} \right\} \end{aligned}$$

Considering the fact that

$$\frac{\partial^2 \mathfrak{A}_\varepsilon}{\partial \sigma_{ij}^2} = \frac{\kappa_\varepsilon}{\sigma_i^2(\sigma_j^2 - \sigma_{ij}^2/\sigma_i^2)^{\frac{3}{2}}} > 0,$$

one can show that when $\sigma_{ij} > 0$, on the surface $\mathbb{W} \cap \{\sigma_i = \sqrt{2\underline{\sigma}}\} \in \mathbb{R}^3$, the following inequality will hold

$$\mathfrak{A}_\varepsilon(\sqrt{2\underline{\sigma}}, \sigma_j, \sigma_{ij}) \leq \mathfrak{A}_\varepsilon(\sqrt{2\underline{\sigma}}, \sigma_j, \min\{\sigma_i\sigma_j, \bar{\sigma}_{\text{cov}}\}).$$

Then, by repeating these steps for $\sigma_i = \sqrt{2\bar{\sigma}}$, $\sigma_j = \sqrt{2\underline{\sigma}}$, $\sigma_j = \sqrt{2\bar{\sigma}}$, and different signs of σ_{ij} , we can show that the extreme values of \mathfrak{A}_ε lands on either surface $(\sigma_i, \sigma_j, \min\{\sigma_i\sigma_j, \bar{\sigma}_{\text{cov}}\})$ or surface $(\sigma_i, \sigma_j, \max\{-\sigma_i\sigma_j, \underline{\sigma}_{\text{cov}}\})$.

In the case when $\sigma_{ij} > 0$, one has $\frac{\partial \mathfrak{A}_\varepsilon}{\partial \sigma_j}|_{\sigma_{ij}=\sigma_{\text{cov}}} < 0$ and $\frac{\partial \mathfrak{A}_\varepsilon}{\partial \sigma_j}|_{\sigma_{ij}=\sigma_{\text{cov}}} < 0$, implying that the upper limit of \mathfrak{A}_ε can only be achieved when $\sigma_j = \sqrt{2\underline{\sigma}}$, such that

$$\begin{aligned} \sup_{(\sigma_i, \sigma_j, \sigma_{ij}) \in \mathbb{W}, \sigma_{ij} > 0} \mathfrak{A}_\varepsilon & < \sup_{\sigma_i \in [\sqrt{2\underline{\sigma}}, \sqrt{2\bar{\sigma}}]} \mathfrak{A}_\varepsilon(\sigma_i, \sqrt{2\underline{\sigma}}, \sigma_i\sqrt{2\underline{\sigma}}) \\ & = \mathfrak{A}_\varepsilon(\sqrt{2\underline{\sigma}}, \sqrt{2\underline{\sigma}}, 2\sqrt{\bar{\sigma}\underline{\sigma}}) \\ & = r(1 - \sqrt{\bar{\sigma}}/\sqrt{\underline{\sigma}}). \end{aligned}$$

In the case when $\sigma_{ij} < 0$, one has $\frac{\partial \mathfrak{A}_\varepsilon}{\partial \sigma_j}|_{\sigma_{ij}=\sigma_{\text{cov}}} > 0$ and $\frac{\partial \mathfrak{A}_\varepsilon}{\partial \sigma_j}|_{\sigma_{ij}=\sigma_{\text{cov}}} < 0$. Considering the fact that $0 > \underline{\sigma}_{\text{cov}} > -2\bar{\sigma}$ despite the value of $|i-j|$, one can show that the upper limit of \mathfrak{A}_ε will be achieved when $\sigma_{ij} = \underline{\sigma}_{\text{cov}} = -\sigma_i\sigma_j$, such that

$$\begin{aligned} \sup_{(\sigma_i, \sigma_j, \sigma_{ij}) \in \mathbb{W}, \sigma_{ij} < 0} \mathfrak{A}_\varepsilon & < \sup_{\sigma_i \in [\sqrt{2\underline{\sigma}}, \sqrt{2\bar{\sigma}}]} \mathfrak{A}_\varepsilon\left(\sigma_i, \frac{|\underline{\sigma}_{\text{cov}}|}{\sigma_i}, \underline{\sigma}_{\text{cov}}\right) \\ & = \mathfrak{A}_\varepsilon\left(\sqrt{2\underline{\sigma}}, \frac{|\underline{\sigma}_{\text{cov}}|}{\sqrt{2\underline{\sigma}}}, \underline{\sigma}_{\text{cov}}\right) \\ & = r(1 - \underline{\sigma}_{\text{cov}}/\sqrt{2\underline{\sigma}}). \end{aligned}$$

Considering the fact that $\underline{\sigma}_{\text{cov}} < 0$, the upper limit of \mathfrak{A}_ε when $\sigma_{ij} < 0$ will be strictly greater than r , indicating the best achievable $\mathcal{A}_\varepsilon^{i,j}$ is always 0 in this case.

In addition to the above scenarios, in the special case when $\sigma_{ij} = 0$, the best achievable risk of cascading collisions boils down to the best achievable risk of single collision as introduced in [27], which solely depends on the value of $\sqrt{2\underline{\sigma}}$. Then, one can conclude by converting the limit of $\mathfrak{A}_\varepsilon(\sigma_i, \sigma_j, \sigma_{ij})$ into the limit of $\mathcal{A}_\varepsilon^{i,j}$. \square

Proof of Corollary 2: Observing the structure of the steady-state covariance terms (Lemma 4), the risk of cascading collision $\mathcal{A}_\varepsilon^{i,j}$ can be considered in two cases based on the value of $|i-j|$. In the case when $|i-j| > 1$, $\mathcal{A}_\varepsilon^{i,j}$ boils down to the risk of single collision, and the best achievable risk can be obtained at $\sigma_j = \sqrt{2\underline{\sigma}}$. In the case when $|i-j| = 1$, \mathfrak{A}_ε can be written as

$$\mathfrak{A}_\varepsilon = \frac{3}{2}r - \frac{1}{2}d^* - \kappa_\varepsilon \sqrt{\frac{3}{4}\sigma_c},$$

where σ_c is shown in Lemma 4. The upper limit of \mathfrak{A}_ε can be obtained as $\sigma_c \rightarrow 2\underline{\sigma}$. Then, one can conclude by converting the limit of $\mathfrak{A}_\varepsilon(\sigma_i, \sigma_j, \sigma_{ij})$ into the limit of $\mathcal{A}_\varepsilon^{i,j}$. \square

REFERENCES

- [1] D. Acemoglu, A. Ozdaglar, and A. Tahbaz-Salehi. “Systemic risk and stability in financial networks”. In: *American Economic Review* 105.2 (2015), pp. 564–608.
- [2] A. Ali, G. Garcia, and P. Martinet. “Enhanced flatbed tow truck model for stable and safe platooning in the presences of lags, communication and sensing delays”. In: *2015 IEEE International Conference on Robotics and Automation (ICRA)*. IEEE. 2015.
- [3] B. Bamieh, M. R. Jovanovic, P. Mitra, and S. Patterson. “Coherence in large-scale networks: Dimension-dependent limitations of local feedback”. In: *IEEE Transactions on Automatic Control* 57.9 (2012), pp. 2235–2249.
- [4] F. Dorfler and F. Bullo. “Synchronization and transient stability in power networks and nonuniform Kuramoto oscillators”. In: *SIAM Journal on Control and Optimization* 50.3 (2012), pp. 1616–1642.
- [5] L. Evans. *An Introduction to Stochastic Differential Equations*. American Mathematical Society, Dec. 2013.
- [6] H. Föllmer and A. Schied. *Stochastic Finance*. De Gruyter, July 2016.
- [7] Y. Ghaedsharaf, C. Somarakis, and N. Motte. “Performance of second-order platoon of vehicles in presence of time-delay and noise”. In: *2018 Annual American Control Conference (ACC)*. IEEE. 2018, pp. 4887–4892.
- [8] R. M. Gray. “Toeplitz and circulant matrices: A review”. In: (2006).
- [9] T. W. Grunberg and D. F. Gayme. “Determining collision potential as a measure of robustness in vehicular networks”. In: *2017 American Control Conference (ACC)*. IEEE. 2017, pp. 3992–3998.
- [10] K. Gu, J. Chen, and V. L. Kharitonov. *Stability of time-delay systems*. Springer Science & Business Media, 2003.
- [11] R. A. Horn and C. R. Johnson. *Matrix analysis*. Cambridge university press, 2012.
- [12] G. Liu, A. Amini, V. Pandey, and N. Motte. “Data-Driven Distributionally Robust Mitigation of Risk of Cascading Failures”. In: *arXiv preprint arXiv:2310.12021* (2023).
- [13] G. Liu, C. Somarakis, and N. Motte. “Emergence of Cascading Risk and Role of Spatial Locations of Collisions in Time-Delayed Platoon of Vehicles”. In: *2022 IEEE 61st Conference on Decision and Control (CDC)*. IEEE. 2022, pp. 6460–6465.
- [14] G. Liu, C. Somarakis, and N. Motte. “Risk of Cascading Failures in Time-Delayed Vehicle Platooning”. In: *2021 60th IEEE Conference on Decision and Control (CDC)*. IEEE. 2021, pp. 4841–4846.
- [15] J. Liu, J. Zhang, and Y. Liu. “Trace inequalities for matrix products and trace bounds for the solution of the algebraic Riccati equations”. In: *Journal of Inequalities and Applications* 2009 (2009), pp. 1–17.

- [16] S. E. A. Mohammed. *Stochastic functional differential equations*. Vol. 99. Pitman Advanced Publishing Program, 1984.
- [17] J. Nocedal and S. J. Wright. *Numerical optimization*. Springer, 1999.
- [18] V. Pandey, G. Liu, A. Amini, and N. Motee. “Quantification of Distributionally Robust Risk of Cascade of Failures in Platoon of Vehicles”. In: *arXiv preprint arXiv:2309.04922* (2023).
- [19] M. Rahnamay-Naeini and M. M. Hayat. “Cascading Failures in Interdependent Infrastructures: An Interdependent Markov-Chain Approach”. In: *IEEE Transactions on Smart Grid* 7.4 (2016), pp. 1997–2006.
- [20] R. T. Rockafellar and S. Uryasev. “Optimization of Conditional Value-at-Risk”. In: *Portfolio The Magazine Of The Fine Arts* 2 (1999), pp. 1–26.
- [21] R. T. Rockafellar and S. Uryasev. “Conditional value-at-risk for general loss distributions”. In: *Journal of Banking and Finance* 26.7 (2002), pp. 1443–1471.
- [22] H. Sandberg, S. Amin, and K. H. Johansson. “Cyberphysical security in networked control systems: An introduction to the issue”. In: *IEEE Control Systems Magazine* 35.1 (2015), pp. 20–23.
- [23] H. Sandberg, V. Gupta, and K. H. Johansson. “Secure networked control systems”. In: *Annual Review of Control, Robotics, and Autonomous Systems* 5 (2022), pp. 445–464.
- [24] S. Sarykalin, G. Serraino, and S. Uryasev. “Value-at-risk vs. conditional value-at-risk in risk management and optimization”. In: *State-of-the-art decision-making tools in the information-intensive age*. Informs, 2008, pp. 270–294.
- [25] M. Siami and N. Motee. “Growing linear dynamical networks endowed by spectral systemic performance measures”. In: *IEEE Transactions on Automatic Control* 63.7 (2017), pp. 2091–2106.
- [26] M. Siami and N. Motee. “Fundamental limits and tradeoffs on disturbance propagation in linear dynamical networks”. In: *IEEE Transactions on Automatic Control* 61.12 (2016), pp. 4055–4062.
- [27] C. Somarakis, Y. Ghaedsharaf, and N. Motee. “Risk of Collision and Detachment in Vehicle Platooning: Time-Delay-Induced Limitations and Tradeoffs”. In: *IEEE Transactions on Automatic Control* 65.8 (2020).
- [28] C. Somarakis, Y. Ghaedsharaf, and N. Motee. “Risk of collision in a vehicle platoon in presence of communication time delay and exogenous stochastic disturbance”. In: *2018 IEEE Conference on Decision and Control (CDC)*. IEEE. 2018, pp. 4487–4492.
- [29] H. Tan, R. Rajamani, and W. Zhang. “Demonstration of an automated highway platoon system”. In: *Proceedings of the 1998 American control conference*. Vol. 3. IEEE. 1998.
- [30] Y. L. Tong. *The multivariate normal distribution*. Springer Science & Business Media, 2012.
- [31] R. A. Usmani. “Inversion of a tridiagonal Jacobi matrix”. In: *Linear Algebra and its Applications* 212.213 (1994), pp. 413–414.
- [32] P. Van Mieghem. *Graph spectra for complex networks*. Cambridge University Press, 2010.
- [33] C. K. Verginis, C. P. Bechlioulis, D. V. Dimarogonas, and K. J. Kyriakopoulos. “Decentralized 2-D control of vehicular platoons under limited visual feedback”. In: *2015 IEEE/RSJ International Conference on Intelligent Robots and Systems (IROS)*. IEEE. 2015.
- [34] C. Wu, A. Kreidieh, K. Parvate, E. Vinitsky, and A. M. Bayen. “Flow: Architecture and benchmarking for reinforcement learning in traffic control”. In: *arXiv preprint arXiv:1710.05465* 10 (2017).
- [35] W. Yu, G. Chen, and M. Cao. “Some necessary and sufficient conditions for second-order consensus in multi-agent dynamical systems”. In: *Automatica* 46.6 (2010), pp. 1089–1095.
- [36] Y. Zhang, A. Arenas, and O. Yağan. “Cascading failures in interdependent systems under a flow redistribution model”. In: *Physical Review E* 97.2 (2018), p. 022307.
- [37] Y. Zhang and O. Yağan. “Robustness of interdependent cyber-physical systems against cascading failures”. In: *IEEE Transactions on Automatic Control* 65.2 (2019), pp. 711–726.
- [38] K. Zhou, J. C. Doyle, and K. Glover. *Robust and optimal control*. 1996.



Guangyi Liu Guangyi Liu received the B.E. degree in aircraft design and engineering from the Beijing Institute of Technology, Beijing, China, in 2016, and the M.S. degree in mechanical engineering in 2018 from the Lehigh University, Bethlehem, PA, USA, where he is currently working toward the Ph.D. degree in robustness and risk analysis of learning and control algorithms in networked systems with the Department of Mechanical Engineering and Mechanics.

His research interests include the risk analysis in perception, networked control systems, and learning systems.



Christoforos Somarakis Christoforos Somarakis received the B.S. degree in Electrical Engineering from the National Technical University of Athens, Athens, Greece, in 2007 and the M.S. and Ph.D. degrees in applied mathematics from the University of Maryland at College Park, in 2012 and 2015, respectively. He was a Post-Doctoral scholar and a Research Scientist with the Department of Mechanical Engineering and Mechanics at Lehigh University from 2016 to 2019. From 2019 until 2022 he was a Member of Research Staff with the Intelligent Systems Lab at Palo Alto Research Center - Xerox. He is currently a Senior Scientist of Mathematical Modelling with the Applied Mathematics Group at Merck & Co.



Nader Motee Nader Motee (Senior Member, IEEE) received the B.Sc. degree in electrical engineering from the Sharif University of Technology, Tehran, Iran, in 2000, and the M.Sc. and Ph.D. degrees in electrical and systems engineering from the University of Pennsylvania, Philadelphia, PA, USA, in 2006 and 2007, respectively. From 2008 to 2011, he was a Postdoctoral Scholar with the Control and Dynamical Systems Department, California Institute of Technology, Pasadena, CA, USA. He is currently a Professor with the Department of Mechanical Engineering and Mechanics, Lehigh University, Bethlehem, PA, USA. His research interests include distributed control systems and real-time robot perception. Dr. Motee was the recipient of several awards including the 2019 Best SIAM Journal of Control and Optimization Paper Prize, the 2008 AACC Hugo Schuck Best Paper Award, the 2007 ACC Best Student Paper Award, the 2008 Joseph and Rosaline Wolf Best Thesis Award, the 2013 Air Force Office of Scientific Research Young Investigator Program Award, 2015 NSF Faculty Early Career Development Award, and a 2016 Office of Naval Research Young Investigator Program Award.